ABSTRACT

Title of dissertation: RESPONSE DYNAMICS OF INTEGRATE-AND-FIRE NEURON MODELS

Joanna Pressley
Doctor of Philosophy, 2008

Dissertation directed by: Professor Todd W. Troyer
Department of Psychology

One of the fundamental problems in neuroscience is characterizing the transfer function that converts noisy synaptic inputs into output firing rates. A common assumption is that the membrane time constant is the dominant factor governing the time course of firing rate responses. However, previous studies have shown that neural response times can be faster than expected from voltage dynamics alone. If the membrane time constant does not determine response time, what are the parameters that describe the transformation of inputs into output firing rates?

We investigate this question using integrate-and-fire models (IF), the simplest neuron models that capture the essential properties of neuronal signaling while remaining simple enough to analyze. Noisy synaptic inputs are modeled as a white noise process with drift, characterized by a time-varying mean and variance. Depending on the baseline levels of the mean and variance of the input, IF models exhibit two basic regimes of neural firing. In the Regular Regime, the drift to threshold is dominant and the neuron produces a regular train of action potentials.

In the Random Regime, the noise in the input dominates and the output is highly variable. We use linear perturbation techniques to analyze the response dynamics of several different IF models, for signals encoded in the mean and the variance of the input, and for models operating in the Regular and Random regimes of behavior.

In the simplest IF model, the perfect integrate-and-fire model (PIF), the sub-threshold membrane dynamics perfectly mimic the integral of the input current. Utilizing linear perturbation techniques, we prove that the model acts like a high-pass filter to variance perturbations and a low-pass filter to perturbations of the mean. Moreover, the sum of the two filters adds perfectly to one. Since changes in the rate of Poisson distributed inputs lead to proportional changes in the mean and variance, these results demonstrate that the PIF produces a perfect replica of the time-varying input rate for Poisson distributed input.

Next we survey the response properties of the leaky integrate-and-fire model (LIF). Our survey covers a wide range of baseline input parameter values as well as for perturbations in either the mean or variance of the input. We find that response dynamics are highly dependent on regime, as well as which input parameter encodes the signal. When the mean level of input is perturbed, the LIF exhibits low-pass behavior. Responses in the Regular Regime display resonances that peak at baseline firing rates. Contrarily, when the input variance is perturbed, the LIF filtering properties are highly regime-dependent, and resonances are found across regimes. Unexpectedly, the resonances do not peak at the underlying firing rate of the model. Many of these response properties can be readily understood by noting that the output firing rate depends on a multiplicative, and hence non-linear

interaction between two factors. One factor is proportional to the present value of the input variance and the other factor depends on past values of both the variance and the mean of the input current.

Additionally we investigate how synaptic dynamics affect LIF response. We model each synaptic input as causing an instantaneous rise and then exponential decay in the total current. This model is the combination of two transformations, one that takes pre-synaptic rates to current and the next that takes current to output firing rates. Considering the entire transformation, the new model is low-pass for both perturbations in the mean as well as the variance. This stems from the low-pass filtering of the transformation from pre-synaptic rates to current. After removing the response properties due to the transformation from pre-synaptic rates to current, we find a striking reduction in the overall gain for variance encoded signals in the Regular Regime. Moreover, the high-frequency gain in the Regular Regime goes to zero, as opposed to one in the previous model. Mean encoded signals elicit responses with finite high-frequency gain across regimes, and reduced resonances.

Finally we focus on nonlinear responses, examining the time course of onset and offset responses for two different IF models, the LIF and the more realistic exponential integrate-and-fire model (EIF). The EIF includes a fast voltage-dependent current active near threshold. In both models, offset responses have a steeper initial slope, but a slower approach to equilibrium. The responses of the models differ in that the EIF shows a slight delay before responding to a step increase in input, a delay that is not found for the LIF nor for the response to step decreases in input for either model.

These results constitute the first systematic exploration of IF dynamics across different qualitative regimes of behavior, focusing on the model and parameters of the input. Our results indicate that the multiplicative form of the expressions derived in these simple models may capture a fundamental nonlinearity governing neural responses to stochastic inputs.

RESPONSE DYNAMICS OF INTEGRATE-AND-FIRE NEURON MODELS

by

Joanna Pressley

Dissertation submitted to the Faculty of the Graduate School of the
University of Maryland, College Park in partial fulfillment
of the requirements for the degree of
Doctor of Philosophy
2008

Advisory Committee:
Professor Todd W. Troyer, Chair/Advisor
Professor Konstantina Trivisa
Professor Howard Elman
Professor Stuart Antman
Professor Elizabeth Quinlan

Dedication

To Chris, my sunshine, my lobster, my love. You fill my life with joy and serenity.

Acknowledgments

I acknowledge that:

Professor Todd Troyer provided me with challenging research problems and trained me to think critically. Todd always made time for me and taught me most of what I know. Thank you Todd for providing invaluable advice and support for the last 6 years.

Chris Pressley supported me (emotionally and financially) while I pursued this degree. Thanks to Chris for babysitting for the last 2 months so I could push to finish. You are what a man should be.

Aviva Pressley made my life more fulfilling and taught me a new meaning for the word love. Thank you Aviva for making getting up everyday easier.

My dad is a feminist. He pushed me to pursue math when other girls were told math was too hard for them. Thank you dad for answering my calls at 4 am when I needed you.

My mom worked fulltime as a teacher and acted as a wonderful role model. Thank you mom for being my bestfriend when I needed one.

My brother Jason developed an interest in math so we would have more to talk about (not that we needed it). Thank you Jason for teaching me to like Ratt.

Professor Konstantina Trivisa is the most positive person I have ever met. Thank you Konstantina for making me feel like I could accomplish anything.

Professor Howard Elman graciously assisted me with my algorithms. Thank you Howard for making time to help me.

Professors Stuart Antman and Elizabeth Quinlan agreed to serve on my committee. Thank you for reading my dissertation.

Professors David Hamilton and Justin Wyss-Gallifent supported my job search and taught me interesting methods of instruction. Thank you for writing me teaching letters of recommendation.

Professors Avis Cohen and Diane O'Leary acted as my mentors. Thank you for supporting me throughout my graduate career.

Professor Ed Saff convinced me to attend graduate school. Thank you Ed for all of the help and advice you have given me.

Alverda McCoy was a joy to be around. Thank you Alverda for helping me jump through the necessary graduate school loops.

Becky and David Colangelo, Amy Wares, and David and Liz Robertson were my DC family. Thank you for making life in DC so much fun.

Justin Brody was a fabulous officemate and friend. Thank you Justin for the enjoyable conversation and for listening to me complain.

Abe Schneider helped me with LaTex and various other odds and ends. Thanks Abe for providing endless IM entertainment.

Ida Sales is the best nanny on the planet. Thank you Ida for loving Aviva so much.

The Math Department provided me with fellowships, teaching assistantships, tuition, travel grants and family health insurance. I was only able to attend graduate school due to this support. Thank you.

Table of Contents

List of Figures

Chapter 1

Introduction

The brain is a complex network containing more than 10^{10} neurons, each of which makes myriad connections with other neurons at physiological structures known as synapses. Neurons transmit information with pulse-like electrical signals called action potentials or spikes. Although the timing of spikes can be very precise in certain brain structures [Rieke et al., 1997, Hutcheon and Yarom, 2000], in the cerebral cortex neuronal spike times are highly irregular [Softky and Koch, 1993]. A dominant hypothesis for how the brain computes in the face of such noise is that information is encoded in the rate of spikes, or firing rate, produced across populations of neurons. Conceptually, the firing rate can be defined as the instantaneous probability that any given neuron will produce a spike, or alternatively as the portion of an ensemble of neurons that spike during a given period of time. To begin to understand dynamic processing in circuits composed of noisy neurons, we must decipher which parameters of the transformation from noisy input to output firing rates determine how quickly neurons respond to changing input.

Our investigation of neural response dynamics focuses on integrate-and-fire neuron models (IF) [Abbott, 1999]. Models of this class are frequently used as building blocks for larger network models, and are the simplest models that contain the basic biological features of neuronal signalling: the integration of subthreshold

inputs by a capacitive cell membrane, a voltage threshold which when reached results in a spike in the membrane potential, and a resetting of the membrane potential to a subthreshold level after the spike. IF models separate the voltage dynamics by timescale. Since action potentials have a stereotyped shape [Rieke et al., 1997] and are fast relative to the slower subthreshold membrane dynamics, the action potential is not described dynamically. Instead when V reaches the threshold level, a spike is recorded, and the membrane potential is reset to a chosen level.

In the most widely used IF model, the leaky integrate-and-fire model (LIF), the slow subthreshold membrane dynamics are given by

$$C\frac{dV}{dt} = g_L(V_L - V) + I_s(t), \tag{1.1}$$

where C is the membrane capacitance, V is the membrane potential, and $I_s(t)$ is the synaptic input current from the pre-synaptic neurons. $g_L(V_L - V)$ is the leak current, which flows through a resistive channel with constant conductance g_L, reversing sign when V equals the reversal potential, V_L. For a fixed input current $I_s(t) = I$, voltage trajectories of equation (1.1) are given as an exponential decay from the initial voltage toward voltage equilibrium $V_\infty = V_L + RI$. The time constant of this decay, $\tau_m = RC$, is known as the membrane time constant and $R = 1/g_L$ is the leak channel resistance. For dynamically changing inputs $I_s(t)$ the voltage trajectory can be calculated as a convolution of the input current with an exponential function with time constant τ_m.

Based on the notion that neural dynamics were dominated by a transformation of inputs to membrane voltage, early researchers created firing rate models based

on simple filtering with a time constant equal to τ_m [Wilson and Cowan, 1973]. However, such models ignore the contribution of crucial nonlinearities to a neuron's response, namely the threshold and resetting of the membrane potential. Indeed, previous research has shown that neural response times can be faster than expected from the voltage time course described by the membrane time constant [Holt et al., 1997, Fourcaud and Brunel, 2002, Silberberg et al., 2004].

In this dissertation, we address the follow general question: *If the firing rate responses of IF models are not determined by the membrane time constant τ_m, what are the parameters that govern neural response dynamics to changing inputs?* Although this is our goal, previous research indicates that this question is under-determined in at least two different ways. First, we must be careful to specify the nature of the input signal. Under the rate coding hypothesis, neurons respond to the combined input from all neurons synapsing on that neuron. Under the assumption that these inputs are independent in time and each individual input results in a voltage change that is small compared with the distance to threshold, we can approximate the total input as a white noise process with a time-varying mean and variance. Note that the mean current for excitatory and inhibitory inputs will subtract while the variance in current contributed by these two inputs will add [Lánský and Sacerdote, 2001]. In the simplest case, keeping the total input rate constant and varying the proportion of excitatory and inhibitory inputs will alter only the mean current whereas adding or subtracting a balanced number of excitatory and inhibitory inputs will alter only the variance. Therefore, in this dissertation, we consider perturbations in both the mean and the variance of the input and study how neural response differs based on

which input parameter is modulated.

A second complicating factor in addressing the general question is that a model with the same set of neural parameters can act very differently based on the baseline input parameter values. There are two extreme regimes of behavior, the Regular and Random Regimes [Abeles, 1991, Troyer and Miller, 1997]. In the Regular Regime, a suprathreshold mean input drives the neuron to spike and the mean period between action potentials is shorter than τ_m. Because of this strong driving force, the neuron acts like an oscillator, producing a regular train of action potentials. Conversely in the Random Regime, the mean driving force is not sufficient to drive the neuron to spike threshold. Rather, action potentials occur when fluctuations randomly accumulate and drive the potential over threshold. The mean period between spikes is typically longer than τ_m and the times between consecutive spikes is highly irregular. Given the qualitatively different nature of spiking in these regimes, we survey neural response over a wide range of baseline input values.

In order to compare IF dynamics across different regimes of model behavior, as well as for encoding signals in both the mean and variance of the input, we take a linear systems approach [Knight, 1972a, Knight, 2000, Nykamp and Tranchina, 2000, Fourcaud and Brunel, 2002]. In doing so, we study the firing rate response due to constant baseline input values plus a sinusoidal perturbation of frequency ω in either the mean or the variance of the input. We decompose the response into the baseline firing rate plus the firing rate component at frequency ω. For small perturbations, the firing rate response to any pattern of input can be reconstructed as a linear combination of these response components. We look at both the amplitude of the

response, or the gain, and the phase shift of the response. Characterizing the linear response in terms of the gain and phase for different modulation frequencies provides a single set of metrics that can be applied across situations.

In chapter 3, we study the response dynamics of the perfect integrate-and-fire model (PIF). Desirable because of its simplicity, the PIF omits leak channels causing a membrane response which is perfectly proportional to the integral of the input current since the last spike. The PIF approximates firing rate response dynamics well when the mean current is large compared to the amount of current needed to drive the voltage to threshold. Here, we utilize diffusion approximation formalism introduced by Gerstein and Mandelbrot in 1964 [Gerstein and Mandelbrot, 1964], which allows the firing rate to be determined from a deterministic PDE, the Fokker-Planck or Forward Kolmogorov equation [Ricciardi, 1977, Risken, 1989, Omurtag et al., 2000, Allen, 2003]. Using FP formalism, we show that if the signal is encoded in both the mean and the variance of the input, the linear response of the PIF is a scaled replica the input.

To study a more realistic model of membrane dynamics, we investigate the response of the LIF model, in chapter 4. Previous researchers have studied the linear response properties of the LIF model for specific sets of input parameters [Brunel et al., 2001, Lindner and Schimansky-Geier, 2001, Fourcaud and Brunel, 2002]. In this chapter, we integrate these disparate results into a comprehensive taxonomy of LIF responses, examining signals encoded in either the mean or the variance of the input, and surveying the linear response over a wide range of baseline parameters. We argue that the key to understanding this taxonomy is the fact that the firing

rate decomposes into a product of two terms. The first term is directly proportional to the input variance. The second term describes the amount of trajectories in a boundary layer near threshold, which is affected by both the mean and the variance of the input.

In chapter 5, we examine how synaptic dynamics affect the response of the LIF. We model synaptic dynamics as a linear transformation from pre-synaptic spike times into current, where each input causes an instantaneous rise and then an exponential decay in the total current. The added complexity of the input adds a second transformation to the model. The new transformation takes input rates to current, and a second transformation takes current to output rates. We make two comparisons with the LIF model having instantaneous inputs. First, we compare the overall transfer function, from input rates to output rates. Next, we divide out the low-pass filtering resulting of the transformation from input rates to current, and compare the transformation from current to output rate with the instantaneous synapse model. As with our other studies, we analyze signals encoded in both the mean and the variance of the input and survey different regimes of behavior.

In chapter 6 we focus on nonlinear responses, examining the time course of the response to the onset and offset of a step change in input. We examine responses for two different IF models: the LIF model discussed above, and the exponential integrate-and-fire model (EIF) in which the leak current is supplemented by a fast, voltage-dependent current meant to mimic the sodium channel dynamics near the onset of the action potential. For both models, offset responses have a steeper initial slope, but a slower approach to equilibrium. In the EIF, but not the LIF

model, onset and offset differ also in that there is a short delay before firing rates change after an increase in input firing rates. Comparing the linear component of the response to square-wave vs. sine-wave inputs indicates that in both models, gain was slightly smaller for square-wave inputs at frequencies above 40 Hz, but phase was relatively unchanged.

Chapter 2

Modeling

2.1 Integrate-and-Fire Model

There are many models of neuronal voltage dynamics, which vary in biological realism and complexity. Integrate-and-fire models (IF), dating back to Lapicque in 1907, capture the essential components of neuronal signaling, while seemingly remaining simple enough to analyze [Abbott, 1999, Burkitt, 2006b, Burkitt, 2006a]. Rather than a single specific model, Integrate-and-fire models are a class of models sharing the following basic assumptions. First, the cell membrane is iso-potential, with a single number describing the membrane voltage. This simplifying assumption focuses the model on the integrative properties of the soma, ignoring the membrane potential gradients that exist in spatially extended dendritic trees. Second, action potentials are triggered when the membrane voltage reaches a specific threshold value. Third, there is a separation of timescales, with fast neuronal dynamics generating stereotyped action potentials. The fast spiking dynamics and the slow membrane integration are assumed to be completely separate, and action potential dynamics are not explicitly modeled. Rather, when threshold is reached, a stereotyped action potential is "pasted" on to the voltage trace and the slow dynamics are suspended for a short refractory period t_{refract}. After the refractory period, the voltage is set to a fixed "reset potential" V_r, and the slow dynamics resumes.

The slow, subthreshold dynamics can be written in general form as

$$C\frac{dV}{dt} = f(V) + I_s(t), \tag{2.1}$$

where C is the membrane capacitance, V is the membrane potential or voltage, and $I_s(t)$ is the external (usually synaptic) current. The form of $f(V)$ distinguishes the different IF models. In some models, action potentials trigger slow time dependent currents that affect membrane integration after a spike [Izhikevich, 2003, Izhikevich, 2004]. These currents, which are modeled by incorporating additional terms on the right hand side of the equation, are not considered here.

The most widely studied IF model is the leaky integrate-and-fire model (LIF):

$$C\frac{dV}{dt} = g_L(V_L - V) + I_s(t), \tag{2.2}$$

where g_L is the leak conductance and V_L is leak channel reversal potential (described below). Leak channels are always open, allowing K^+, Na^+ and Cl^- ions to flow through the membrane. Many more leak channels are selective for K^+ than for Na^+ or Cl^- (figure 2.1). There are two forces acting on the ions which determine whether they flow through the membrane. The first force is the electromotive force, determined by the present value of the membrane potential. An energy consuming pump maintains the resting potential of the membrane at around $-70\ mV$ and keeps the quantity of K^+ cells larger on the inside than outside and Na^+ cells larger on the outside than inside. Since the membrane potential is negative, the electromotive force will draw the positively charged ions into the cell and repel the negatively charged ions. The other force is diffusive and due to the chemical

gradient. Overall, these forces combine to produce the reversal potential of the leak channels V_L, at which the direction of ion flow switches.

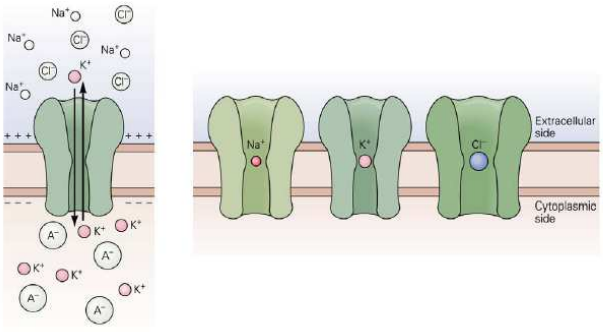

Figure 2.1: From Kandel and Schwartz [Kandel et al., 2000]. Leak channels allow K^+, Na^+ and Cl^- ions to flow through the membrane. Channels are selective for each ion type.

It is common to divide through by the leak conductance and write the model as

$$\tau_m \frac{dV}{dt} = -V + V_L + RI(t). \tag{2.3}$$

In this form, it is clear that for constant input, the voltage decays exponentially to a voltage $V_\infty = V_L + RI$ with a time constant $\tau_m = RC$. Here, $R = 1/g_L$ is the leak channel resistance. This model is studied in chapters 4, 5 and 6.

In this thesis we also consider two other IF models. In chapter 3, we analyze the simplest IF model, the perfect integrate-and-fire model (PIF). The PIF model contains no intrinsic currents and the membrane voltage is proportional to

the integral of the input current since the time t_{sp} at the end of the last spike:

$$C\frac{dV}{dt} = I(t) \tag{2.4}$$

$$V(t - t_{sp}) = V_{reset} + \frac{1}{C}\int_{t_{sp}}^{t} I(t')dt'. \tag{2.5}$$

The lack of intrinsic currents simplifies the dynamics and allows closed form expressions to be derived in some cases [Knight, 1972a, Abbott and van Vreeswijk, 1993, Fourcaud and Brunel, 2002] and see chapter 3. The behavior of this model approximates that of the LIF model when input currents are strong and excitatory, driving the membrane potential monotonically toward threshold at rates significantly faster than $1/\tau_m$.

In chapter 6, along with the LIF, we study the exponential integrate-and-fire model (EIF) [Fourcaud-Trocmé et al., 2003, Fourcaud-Trocmé and Brunel, 2005]. The EIF's peri-threshold voltage dynamics more closely match models containing a sodium current whose activation triggers the onset of an action potential. The model consists of the leak channels plus an instantaneous voltage-dependent spiking current $\psi(V)$ that is only activated for voltages near threshold:

$$C\frac{dV}{dt} = g_L(V_L - V) + \psi(V) + I(t) \tag{2.6}$$

$$\psi(V) = g_L\Delta_T \exp\left(\frac{(V-\theta)}{\Delta_T}\right). \tag{2.7}$$

Δ_T is the "spike slope factor" which determines the voltage sensitivity of the spiking current. θ is the voltage threshold at which the slope of the I-V curve, which describes the intrinsic currents versus the membrane potential, vanishes and the equation becomes unstable. Conceptually, spikes are triggered at the time at which

voltage diverges to infinity. Practically, the time at which voltage crosses a triggering threshold (= -30 mV) is recorded, and the time from -30 mV to infinity is calculated analytically, by assuming the noise is negligible once the intrinsic current is highly activated. After the spike, the voltage is reset immediately to $V_r = -68\ mV$, and voltage integration resumes after waiting for a refractory period $t_{\text{refract}} = 1.7$ msec.

2.2 Stochastic Input Model

The majority of the studies in this thesis consider "instantaneous synapses", where the synaptic input consists of a series of instantaneous pulses of current:

$$I_s(t) = \sum_k \overline{Q}\delta(t - t^k). \tag{2.8}$$

Here, $\overline{Q}$ is the total charge carried by one input and t^k is the arrival time of the kth pre-synaptic spike. The arrival times follow a Poisson process with average rate $\lambda(t)$. Inputs are pulse like and are modeled by $\delta(t - t')$, the Dirac delta function. $\delta(t - t')$ is zero everywhere except $t = t'$, and has an integral of 1 in time.

The current is a stochastic process whose mean at any time is given by $\mu(t) = \overline{Q}\lambda(t)$. The input spike train is a Poisson process, with a variance given by $\lambda(t)$. Since each input has size $\overline{Q}$, the variance of the current is $\overline{Q}^2\lambda(t)$, which has units $nC^2/msec$. This can be thought of as the accumulation of the variance of the charge over time.

If synaptic inputs are instantaneous, weak, and uncorrelated in time, we can adopt a diffusion approximation, and write the input current $I_s(t)$ as

$$I_s(t) = \mu(t) + \sigma(t)\eta(t). \tag{2.9}$$

$\mu(t) = \overline{Q}\lambda(t)$ is the mean current, $\sigma(t) = \overline{Q}\sqrt{\lambda(t)}$, and $\eta(t)$ is Gaussian white noise process ($\langle\eta(t)\rangle = 0$ and $\langle\eta(t)\eta(t')\rangle = \delta(t-t')$) [Brunel and Hakim, 1999, Knight, 2000, Fourcaud and Brunel, 2002, Silberberg et al., 2004]. Therefore, we consider the stochastic differential equation:

$$C\frac{dV}{dt} = f(V) + \mu(t) + \sigma(t)\eta(t), \tag{2.10}$$

where $f(V) = g_L(V_L - V)$ for the LIF, $f(V) = 0$ for the PIF, and $f(V) = g_L(V_L - V) + \psi(V)$ for the EIF.

2.2.1 Numerical Simulations

In chapter 6, we rely on direct simulation of the SDE (2.10) to compare the responses of the LIF and EIF. First, we specify a fixed time course for the mean $\mu(t)$ and variance $\sigma^2(t)$ of the stochastic input. A particular voltage path is obtained by numerically solving equation (2.10) until the voltage reaches threshold and then resetting the voltage to the chosen reset level, repeatedly for the length of the trial. Firing rates are determined by forming the peri-stimulus time histogram (PSTH) of spike times obtained from repeated trials (on the order of 750,000) using different noise seeds. The post-synaptic firing rate is estimated by calculating the probability of having a spike in each small time bin of the PSTH (bins usually 1 msec wide).

To numerically solve equation (2.10), we use a 2nd order Stochastic Runge-Kutta method engineered by Honeycutt [Honeycutt, 1992]. All simulations are performed using MATLAB (Mathworks, Natick, MA). Step size is taken as $dt = 2^{-4} = 0.0625$ msec, and noise currents $\eta(t)$ are assumed constant over each time step. The

amplitudes of these currents are chosen from a zero-mean Gaussian distribution with standard deviation equal to $\sigma = 2\mu A\sqrt{msec}/cm^2$ [Fourcaud-Trocmé et al., 2003]. To more accurately simulate the rapid spike dynamics in the EIF model, during any time step in which voltage went above the voltage threshold, θ, the dynamics are re-simulated using a reduced time step of $1/5 * 2^{-4} = 0.0125$ msec. (Noise currents are still assumed constant over the larger 2^{-4} msec time step.)

The LIF model uses identical parameters, except $\psi(V) = 0$. A spike is registered immediately when the voltage reached spike threshold, set at $\theta = -59.9$ mV. We find that by adding a 3.5 msec refractory period, the LIF's f-I curve, which plots the steady-state firing rate as a function of current, matched that of the EIF model surprisingly well. The refractory period is implemented by resetting voltage to $V_r =$ -68 mV, waiting 3.5 msec after the spike, and then resuming integration according to the LIF SDE.

2.2.2 Fokker-Planck Formalism

Instead of directly tracking individual trajectories with the stochastic differential equation (2.10), in chapters 3 and 4 we use the Fokker-Planck (forward Kolmogorov) formalism to study the dynamics of the probability density function over voltage, $\rho(V, t)$ [see Appendix for derivation] [Arnold, 1974, Ricciardi, 1977, Risken, 1989, Brunel and Hakim, 1999, Fourcaud and Brunel, 2002, Allen, 2003].

$\rho(V, t)$ represents the probability that a given trajectory is near the voltage V at time t. For any given voltage the net flux or "rate of flow" $J_V(V, t)$ across that

voltage can be calculated as

$$J_V(V,t) = -\frac{R^2\sigma^2(t)}{2\tau_m^2}\frac{\partial\rho(V,t)}{\partial V} + \frac{V_L - V(t) + R\mu(t)}{\tau_m}\rho(V,t). \tag{2.11}$$

The probability density obeys the following dynamics:

$$\tau_m\frac{\partial\rho(V,t)}{\partial t} = \tau_m\ \frac{-\partial J_V(V,t)}{\partial V} \tag{2.12}$$

$$= \frac{R^2\sigma^2(t)}{2\tau_m}\frac{\partial^2\rho(V,t)}{\partial V^2} - \frac{\partial}{\partial V}[V_L - V(t) + R\mu(t)]\rho(V,t). \tag{2.13}$$

The first term on the right-hand side is the diffusion term, which describes how the ensemble's voltage distribution spreads out due to noise, and the second term is the drift or driving force, which describes how the mean input and leak forces affect the distribution.

For the Fokker-Planck equations, boundary conditions are imposed to account for the voltage threshold and reset. The threshold condition is modeled as an absorbing boundary imposed at the threshold θ, and the firing rate is simply the flux crossing threshold, $r(t) = J_V(\theta,t)$. This probability flux is then re-injected at voltage reset [Brunel and Hakim, 1999, Brunel, 2000, Fourcaud and Brunel, 2002]. More specifically, the boundary conditions are as follows:

1. Under the standard diffusion approximation, the density must be equal to zero at an absorbing boundary, lest the flux becomes infinite [Brunel, 2000]. Therefore,

$$\rho(\theta,t) = 0. \tag{2.14}$$

2. The firing rate is given as the flux across threshold:

$$r(t) = J_V(\theta,t) = \frac{R^2\sigma^2(t)}{2\tau_m^2}\left(-\frac{\partial\rho}{\partial V}(\theta,t)\right). \tag{2.15}$$

3. The probability density that crosses threshold is injected back at the reset voltage V_r. To conserve the total flux, the flux leaving V_r from the right, $J_V(V_{r_+}, t)$, must be equal to the sum of the firing rate plus the flux arriving from the left, $J_V(V_{r_-}, t) + r(t)$. That is,

$$J_V(V_{r_+}, t) - J_V(V_{r_-}, t) = r(t). \tag{2.16}$$

4. The final condition imposed is that the total probability must remain at unity:

$$\int_{-\infty}^{\theta} \rho(V, t) dV = 1. \tag{2.17}$$

2.2.3 Numerical Solution of the Fokker-Planck Model

When simulating the Fokker-Planck equation, firing rate responses are determined using numerical simulation of equations (2.13) and (2.15). We use the Crank-Nicholson method in time and central differencing in voltage as approximations to the derivatives [Vreugdenshil, 1989, Larsson and Thomée, 2003]. The resulting linear system has the form $A\rho^{t+dt} = B\rho^t$ where A and B are tridiagonal except for one other nonzero pixel due to the resetting of the flux over threshold. The three nonzero diagonals are caused by central differencing, which approximates the derivatives at any voltage in the FP equation using weighted values of itself and the voltages to directly to the left and right. Except for small and large frequency modulations, the voltage bin $dv = 2^{-2} = 0.25$ mV, while the the time bin $dt = 2^{-6} = 0.015625$ $msec$.

The final condition imposed is that the total probability, $\int_{-\infty}^{\theta} \rho(V, t) dV$, must equal unity is used to set initial conditions and to solve for the firing rate. To obtain the firing rate, we first solve $A\rho^{t+dt} = B\rho^t$ for ρ^{t+dt}. Then the integral of

$\rho(V, t + dt)dV$ is approximated using the trapezoidal rule, with each bin having area of width dv and height measured as the average of the height of the density endpoints. To rectify the numerical problem of having an infinite left boundary, the density is forced to zero and an absorbing boundary is placed at $-90\ mV$, where the density was known from pilot simulations to be nearly zero. Since without the boundary conditions the discretization would conserve volume, the flux is then determined by how much area is lost from the left and right (threshold) boundaries. Any flux passing over the left boundary is replaced into the first voltage bin above that boundary. The flux over threshold is replaced into the voltage reset bin.

To compare LIF dynamics across the regimes of model behavior, we take a linear systems approach, measuring the gain and phase of the response to sinusoidal perturbations in the input parameters $\mu(t)$ and $\sigma^2(t)$. We use the subscript '0' to denote the baseline value of the parameter (the '0th' harmonic), and the subscript '1' to denote the amplitude of the sinusoidal modulation (the 1st harmonic). To cover all regimes of model behavior, we vary the baseline level of mean input μ_0 between 0.5 $\mu A/cm^2$ and 2.5 $\mu A/cm^2$ in 0.125 $\mu A/cm^2$ steps, and the baseline variance σ_0^2 between 0.4 $\mu A^2 msec/cm^4$ and 3 $\mu A^2 msec/cm^4$ in steps of 0.1 $\mu A^2 msec/cm^4$. The mean and variance of the input are modulated separately, varying one parameter while holding the other constant. At each combination of these baseline parameters, we ran simulations in which we added small amplitude sinusoidal modulations across a range of input frequencies ω ($\mu(t) = \mu_0 + \mu_1 \cos(\omega t)$ or $\sigma^2(t) = \sigma_0^2 + \sigma_1^2 \cos(\omega t)$). For the initial survey, we examine the frequencies $0.5Hz \leq \omega \leq 500Hz$. In several cases, we examine higher frequency responses (up to 10,000 Hz). These cases include

determining the high-frequency response for a subset of total baseline parameter space and determining cutoff frequencies for mean perturbations.

2.3 LIF Model - Equation of Order Two

In addition to instantaneous synapses, we study a model in which synaptic currents have a finite timescale. In this more realistic model, each pre-synaptic spike causes the release of an instantaneous pulse of neurotransmitter. The neurotransmitter binds with receptors on the post-synaptic membrane causing the associated channels to open and ions to flow through. We assume that neurotransmitter becomes unbound from post-synaptic receptors at a fixed rate, leading to an exponential decay in the number of bound receptors with decay constant τ_s [Destexhe et al., 1998, Brunel and Sergi, 1998, Haskell et al., 2001]. The dynamics of this process are

$$\frac{dB}{dt} = \frac{-B(t)}{\tau_s} + \sum_{t_k} N\delta(t - t_k), \tag{2.18}$$

where B is the number of bound receptors at time t, N is the peak number of bound receptors for each pulse of transmitter, and t_k are the arrival times of a train of presynaptic spikes. If we consider a single input arriving at time t', the average number of bound receptors is given by

$$B(t) = Ne^{\frac{-(t-t')}{\tau_s}}\Theta(t'), \tag{2.19}$$

where $\Theta(t')$ represents the Heaviside function. Assuming each receptor yields a current $\widehat{I}$, the input current from the single input at any time, $I(t)$, is given by

$$I(t) = \widehat{I}B = \widehat{I}Ne^{\frac{-(t-t')}{\tau_s}}\Theta(t'). \tag{2.20}$$

If we let the peak current be $\overline{I} = \widehat{I}N$, we note that each input contributes a total charge of $\overline{Q} = \overline{I}\tau_s = \widehat{I}N\tau_s$.

Applying the diffusion approximation to the event arrival times in this model, we let $\mu_s(t)$ (spikes/time) be the mean number of pre-synaptic spikes per time, and $\sigma_s^2(t)$ $(spikes^2/time)$ be the variance of the number of spikes per time. Then equation (2.18) becomes

$$\tau_s \frac{dB}{dt} = -B(t) + \tau_s N\mu_s(t) + \tau_s N\sigma_s(t)\eta(t), \tag{2.21}$$

where $\eta(t)$ is a unit variance white noise process. Multiplying through by $\widehat{I}$, and using $I(t) = \widehat{I}B$ we find:

$$\tau_s \frac{dI_s}{dt} = -I_s(t) + \widehat{I}\tau_s N\mu_s(t) + \widehat{I}\tau_s N\sigma_s(t)\eta(t) \tag{2.22}$$

$$= -I_s(t) + \overline{Q}\mu_s(t) + \overline{Q}\sigma_s(t)\eta(t). \tag{2.23}$$

If we let $\mu(t) = \overline{Q}\mu_s(t)$ and $\sigma(t) = \overline{Q}\sigma_s(t)$ then we get

$$\tau_s \frac{dI_s}{dt} = -I_s(t) + \mu(t) + \sigma(t)\eta(t) \tag{2.24}$$

[Brunel et al., 2001, Fourcaud and Brunel, 2002, Moreno-Bote and Parga, 2004].

In chapter 5, we study (2.3) when the synaptic input is given by equation (2.24). The following system of equations tracks the current evolution and the sub-threshold membrane dynamics [Fourcaud and Brunel, 2002]:

$$C\frac{dV}{dt} = \frac{1}{R}(V_L - V) + I_s(t) \tag{2.25}$$

$$\tau_s \frac{dI_s}{dt} = -I_s + \mu(t) + \sigma(t)\eta(t). \tag{2.26}$$

We call this the 2D LIF model since the state space for the coupled differential equations (2.25) and (2.26) yield a two-dimensional state space.

2.3.1 Fokker-Planck for the 2D Model

For the 2D LIF neuron model, the probability density $\rho(V, I_s)$ is a function of both the voltage and synaptic current. The flux in the current direction is given by

$$J_{I_s}(V, I_s, t) = \frac{-1}{\tau_s}\left[\frac{\sigma^2}{2\tau_s}\frac{\partial \rho}{\partial I_s} + (I_s - \mu)\rho(V, I_s)\right] \tag{2.27}$$

and the flux in the voltage direction is

$$J_V(V, I_s, t) = \frac{(RI_s + V_L - V)\rho}{\tau_m}. \tag{2.28}$$

Changes in the probability density depend on the sum of the partial derivatives of the flux in these two directions:

$$\frac{\partial \rho}{\partial t} = -\frac{\partial}{\partial I_s}J_{I_s} - \frac{\partial}{\partial V}J_V \tag{2.29}$$

$$= \frac{1}{\tau_s}\left[\frac{\sigma^2}{2\tau_s}\frac{\partial^2 \rho}{\partial I_s^2} + \frac{\partial}{\partial I_s}(I_s - \mu)\rho\right] - \frac{1}{\tau_m}\frac{\partial}{\partial V}(RI_s + V_L - V)\rho. \tag{2.30}$$

The flux over threshold for a given level of input current I_s is

$$J_V(\theta, I_s, t) = \Theta(RI_s(t) + V_L - \theta)\frac{(RI_s(t) + V_L - \theta)\rho}{\tau_m}, \tag{2.31}$$

where the Heaviside function Θ captures the fact that there is no flux across threshold when the net current is negative. The flux over threshold is re-injected at voltage reset in a manner that conserves total flux:

$$J_V(V_{r+}, I_s, t) = J_V(\theta, I_s, t) + J_V(V_{r-}, I_s, t). \tag{2.32}$$

The firing rate is then calculated as the summed flux over all current values:

$$r(t) = \int_{-\infty}^{\infty} J_V(\theta, I_s, t) dI_s. \tag{2.33}$$

The boundary conditions for this system are simply the conditions that bound the probability density [Fourcaud and Brunel, 2002]:

$$\lim_{I_s \to \pm\infty} J_{I_s}(V, I_s, t) = 0 \tag{2.34}$$

$$\lim_{V \to -\infty} J_V(V, I_s, t) = 0, \tag{2.35}$$

plus the condition that total probability density is conserved. Note that because there is no diffusion in the voltage direction, $\rho(V, I_s, t)$ can take on finite values for $V = \theta$.

2.4 Numerical Simulations for the 2D Model

Numerical solutions are calculated for a two dimensional rectangular grid with a spacing of 0.5 mV in the voltage direction and 0.5 $\mu A/cm^2$ in the current direction. The domain in the continuous case is $(-\infty, \infty)$ for I_s and $(-\infty, \theta)$ for V. We know that $\lim_{I_s \to \pm\infty} \rho(V, I_s, t) = 0$ and $\lim_{V \to -\infty} \rho(V, I_s, t) = 0$. So we bound I_s from above and below and V from below by values where from pilot simulations we knew the density would be nearly zero. These values are dependent on σ_0^2 and τ_s and range from $-5\mu A/cm^2$ to $6\mu A/cm^2$ for I_s and $-78mV$ to $-71mV$ for V. Any flux over the I_s boundaries is re-inserted at the point right above or below the boundary. Any flux over the left V boundary is re-inserted at the point to the right of the boundary. The density at the boundaries is forced to exactly zero.

For the 2D model, we use Euler's method or if that is not stable, Crank-Nicholson, as an approximation to the derivative $\frac{\partial \rho}{\partial t}$ and central differencing for the derivatives $\frac{\partial \rho}{\partial I_s}$ and $\frac{\partial^2 \rho}{\partial I_s^2}$. Given the lack of diffusion in the voltage parameter, central

differencing for the voltage derivatives causes oscillations in the solutions. Therefore, we use a mixed forward/backward differencing scheme for the derivative in voltage. The direction of forcing is determined by the total current $I(I_s, V) = RI_s + V_L - V$. For positive net current, $I > 0$, the voltage flux is determined by the flow from lower voltage values. Therefore, we use backward differencing in this region. For negative net currents, $I < 0$ the flux is determined by the flow from higher voltage values, so we use forward differencing. Finally, to conserve volume, the voltage flux at the points where $I = 0$ is taken as the sum from the left and right. The grid is arranged so that for each I_s value there is a voltage at which $I = 0$.

The firing rate is calculated as the amount of density flux over threshold. Flux over threshold only occurs for values of $I > 0$ and is calculated as the volume not conserved by the backward differencing scheme. We approximate volume as the sum of the volume above each voxel on the grid. The height above each voxel was approximated as the average of the two density values at the right corners, thinking of voltage as going from left to right and current going from bottom to top. The right values are used so that firing rate was only dependent on the density at threshold.

Chapter 3

PIF Response to Stochastic Input Rates

The focus of this chapter is determining the linear response properties of the perfect integrate-and-fire neuron model (PIF) when the input is modeled by a white noise process plus drift. The simplest of the IF models, the PIF omits leak channels causing the membrane voltage to be perfectly proportional to the integral of the input current since the last spike.

PIF response to deterministic sinusoidal input was determined by Knight in his seminal work from 1972 [Knight, 1972a]. Knight first discussed the single neuron PIF response, defined as the inverse of the interval between two spikes. Utilizing linear perturbation theory, he then derived the PIF response to small sinusoidal perturbations of the input current. He found that the response perturbation was proportional to the input perturbation averaged over an interval whose length was equal to the baseline inter-spike interval, T_0. This averaging caused the PIF to act as a low-pass filter and for the gain to go to zero when the period of the sinusoidal input was a multiple of T_0 (figure 3.1). Knight then described the firing rate response of a large population of PIF neurons, proportional to the fraction of the population firing at any given time. Again using linear perturbation theory, Knight exhibited that in contrast to the single neuron response, the population response was an exact scaled replica of the input signal.

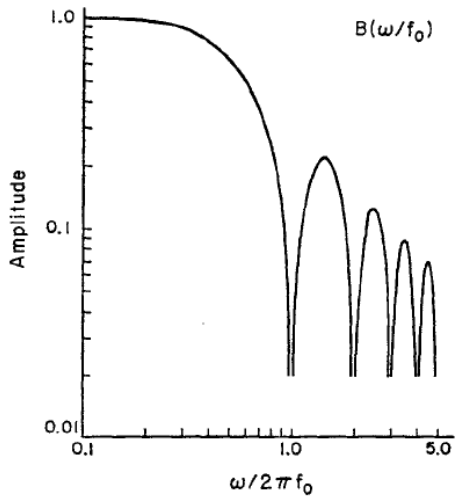

Figure 3.1: From Knight 1972 [Knight, 1972a]. Single unit response to sinusoidal modulations in the signal. PIF acts like a low-pass filter with amplitude going to zero at multiples of the steady state firing rate, f_0

More recently, Fourcaud and Brunel furthered Knight's work by studying PIF response to stochastic white noise inputs, using methods introduced by Gerstein and Mandelbrot [Gerstein and Mandelbrot, 1964, Fourcaud and Brunel, 2002]. Fourcaud and Brunel showed that the linear response to sinusoidal perturbations in the mean input current was low-pass, dropping to zero for input modulations significantly faster than σ^2/μ^2, where σ^2 is the variance and μ is the mean of the input at baseline.

But changes in the pre-synaptic firing rate will cause changes in both the mean *and* the variance of the input current. For example, for Poisson-distributed pre-synaptic spike trains, changes in the variance of the current are proportional to changes in the mean. To reconstruct the linear response to changes in input rates, we therefore derive the linear response properties for modulations of the input variance. Combining these results with Fourcaud and Brunel's, we find that for small modulations in the Poisson input rate, the PIF population response is a scaled replica of the input, mirroring Knight's original result for deterministic input.

3.1 Perturbations of the Variance

Previous work has produced solutions of the PIF when μ and σ are held constant [Abbott and van Vreeswijk, 1993], as well as for solutions of the dynamical probability density function due to sinusoidal perturbations in the mean of the synaptic input [Fourcaud and Brunel, 2002]. Here we extend the derivation of Fourcaud and Brunel (2002) to examine the firing rate response of the PIF to sinusoidal

perturbations in the input variance. As a stochastic differential equation, the PIF is written as

$$C\frac{dV}{dt} = \mu(t) + \sigma(t)\eta(t). \tag{3.1}$$

Using the Fokker-Planck formalism (see Methods),

$$C\frac{\partial \rho}{\partial t} = \frac{\sigma^2}{2C}\frac{\partial \rho^2}{\partial^2 V} - \mu\frac{\partial \rho}{\partial V}. \tag{3.2}$$

We examine the response dynamics of the PIF when the input variance is perturbed by sinusoids of frequency ω (complex notation is used to simplify calculations):

$$\sigma^2(t) = \sigma_0^2(1 + \epsilon e^{i\omega t}). \tag{3.3}$$

To simplify notation, we make the following change of variables:

$$u = \frac{2\mu_0 VC}{\sigma_0^2},\ u_\theta = \frac{2\mu_0 \theta C}{\sigma_0^2},\ u_r = \frac{2\mu_0 V_r C}{\sigma_0^2},\ \tau_e = \frac{\sigma_0^2}{2\mu_0^2}. \tag{3.4}$$

After making these change of variables the Fokker-Planck equation becomes

$$\tau_e\frac{\partial \rho(u,\omega)}{\partial t} = (1 + \epsilon e^{i\omega t})\frac{\partial \rho^2}{\partial^2 u} - \frac{\partial \rho}{\partial u}. \tag{3.5}$$

Note that σ_0^2 has units of charge^2/time and μ has units of charge/time. Therefore, the ratio of the variance to mean squared sets a characteristic timescale τ_e for the PIF.

The boundary conditions (see methods) in the new variables are:

- The density is equal to zero at an absorbing boundary (threshold) to prevent an infinite flux:

$$\rho(u_\theta, t) = 0. \tag{3.6}$$

- Similarly, the density must be continuous at the reset potential to prevent an infinite flux:

$$\rho(u_{r_-}, t) = \rho(u_{r_+}, t). \tag{3.7}$$

- The firing rate is given as the flux across threshold:

$$\frac{d\rho}{du}(u_\theta, t) = -r(t)\tau_e. \tag{3.8}$$

- The firing rate is injected back at the reset voltage V_r:

$$\frac{d\rho}{du}(u_{r_+}, t) - \frac{d\rho}{du}(u_{r_-}, t) = -r(t)\tau_e. \tag{3.9}$$

- The integrated probability is equal to one:

$$\int_{-\infty}^{\theta} \rho(u, t)du = 1. \tag{3.10}$$

To characterize the perturbations to the output, $\rho(u, \omega, t)$ and $r(t)$ are expanded in terms of a small parameter ϵ:

$$\rho(u, \omega, t) = \rho_0(u) + \epsilon e^{i\omega t}\widehat{\rho}(u, \omega) + O(\epsilon^2) \tag{3.11}$$

$$r(t) = r_0(1 + \epsilon e^{i\omega t}\widehat{n}(\omega)) + O(\epsilon^2). \tag{3.12}$$

After plugging (3.11) into (3.5) we separate the terms into two equations, the steady-state equation and the 1st order equation, which describes the PIF response to the sinusoidal component of variance.

The steady state solution is given by [Abbott and van Vreeswijk, 1993]

$$\rho_0 = r_0\tau_e[1 - e^{u-u_\theta} - \Theta(u_r - u)(1 - e^{u-u_r})]. \tag{3.13}$$

Note that $\frac{\partial^n \rho_0}{\partial u^n} = \frac{\partial \rho_0}{\partial u}$ for $n > 1$.

The 1st order equation is a nonhomogeneous ordinary differential equation:

$$i\tau_e \omega \widehat{\rho} = \frac{d^2 \rho_0}{du^2} + \frac{d^2 \widehat{\rho}}{du^2} - \frac{d\widehat{\rho}}{du}. \tag{3.14}$$

The boundary conditions for the 1st order equations are:

$$\widehat{\rho}(u_\theta) = 0 \tag{3.15}$$

$$\widehat{\rho}(u_{r_+}) = \widehat{\rho}(u_{r_-}) \tag{3.16}$$

$$\left(\frac{\partial \rho_0}{\partial u}(u_\theta) + \frac{\partial \widehat{\rho}}{\partial u}(u_\theta, \omega) \right) = -r_0 \widehat{n}(\omega) \tau_e \tag{3.17}$$

$$\frac{\partial \rho_0}{\partial u}(u_{r_+}) - \frac{\partial \rho_0}{\partial u}(u_{r_-}) + \frac{\partial \widehat{\rho}}{\partial u}(u_{r_+}, \omega) - \frac{\partial \widehat{\rho}}{\partial u}(u_{r_-}, \omega) = -r_0 \widehat{n}(\omega) \tau_e \tag{3.18}$$

$$\int_{-\infty}^{\theta} \widehat{\rho}(u, \omega) du = 0. \tag{3.19}$$

The solution is determined by finding the general solution to the corresponding homogeneous equation and adding to this a particular solution $\widehat{\rho}_p$. First we guess that the particular solution has the form $\widehat{\rho}_p = K \frac{\partial \rho_0}{\partial u}$, due to the particular solution for mean perturbations [Fourcaud and Brunel, 2002]. Plugging $\widehat{\rho}_p = K \frac{\partial \rho_0}{\partial u}$ into (3.14):

$$i\tau_e \omega K \frac{\partial \rho_0}{\partial u} = \frac{\partial \rho_0}{\partial u} + K \frac{\partial \rho_0}{\partial u} - K \frac{\partial \rho_0}{\partial u}. \tag{3.20}$$

So $K = \frac{1}{i\omega\tau_e}$ and $\widehat{\rho}_p = \frac{1}{i\omega\tau_e} \frac{\partial \rho_0}{\partial u}$.

Next we find the general solution of the homogeneous ODE:

$$\frac{d^2 \widehat{\rho}}{du^2} - \frac{d\widehat{\rho}}{du} - i\tau_e \omega \widehat{\rho} = 0. \tag{3.21}$$

We assume that the solution is of the form e^{zu}, and find:

$$z^2 - z - i\omega\tau_e = 0 \tag{3.22}$$

$$z \pm (\omega) = \frac{1 \pm \sqrt{1 + 4i\omega\tau_e}}{2}. \tag{3.23}$$

After some algebra (Appendix A.2.1), we find that the solution for $\widehat{\rho}$ is

$$\widehat{\rho} = \frac{r_0}{i\omega}[-e^{u-u_\theta} + \Theta(u_r - u)(e^{u-ur}) + e^{z_+(\omega)(u-u_\theta)} - \Theta(u_r - u)e^{z_+(\omega)(u-u_r)}] \tag{3.24}$$

and from the boundary conditions, the solution for the firing rate modulations $\widehat{n}(\omega)$ is

$$\widehat{n}(\omega) = 1 - \frac{\sqrt{1 + 4i\omega\tau_e} - 1}{2i\omega\tau_e}. \tag{3.25}$$

3.2 Perturbations of the Mean

The derivation of the first order response to modulations in the mean is similar [Fourcaud and Brunel, 2002]. Letting

$$\mu(t) = \mu_0(1 + \epsilon e^{i\omega t}), \tag{3.26}$$

the Fokker-Planck equation in the transformed coordinates is

$$\tau_e \frac{\partial \rho(u,\omega)}{\partial t} = \frac{\partial \rho^2}{\partial^2 u} - (1 + \epsilon e^{i\omega t})\frac{\partial \rho}{\partial u}. \tag{3.27}$$

Breaking out the first order terms, we arrive at the nonhomogeneous differential equation:

$$i\tau_e\omega\widehat{\rho} = \frac{d^2\widehat{\rho}}{du^2} - \frac{d\widehat{\rho}}{du} - \frac{d\rho_0}{du}. \tag{3.28}$$

Again, we assume the particular solution has the form $\widehat{\rho}_p = K\frac{\partial\rho_0}{\partial u}$, and find

$$i\tau_e\omega K\frac{\partial\rho_0}{\partial u} = K\frac{\partial\rho_0}{\partial u} - K\frac{\partial\rho_0}{\partial u} - \frac{\partial\rho_0}{\partial u}, \tag{3.29}$$

which yields and $\widehat{\rho}_p = \frac{-1}{i\omega\tau_e}\frac{\partial\rho_0}{\partial u}$. Again trying solutions of the form e^{zu} to the corresponding homogeneous equation:

$$\frac{d^2\widehat{\rho}}{du^2} - \frac{d\widehat{\rho}}{du} - i\tau_e\omega\widehat{\rho} = 0 \tag{3.30}$$

we find

$$z^2 - z - i\omega\tau_e = 0 \tag{3.31}$$

$$z \pm (\omega) = \frac{1 \pm \sqrt{1 + 4i\omega\tau_e}}{2}. \tag{3.32}$$

The following equations replace boundary conditions (3.17) and (3.18):

$$\frac{\partial\widehat{\rho}}{\partial u}(u_\theta, \omega) = -r_0\widehat{n}(\omega)\tau_e \tag{3.33}$$

$$\frac{\partial\widehat{\rho}}{\partial u}(u_{r_+}, \omega) - \frac{\partial\widehat{\rho}}{\partial u}(u_{r_-}, \omega) = -r_0\widehat{n}(\omega)\tau_e. \tag{3.34}$$

Using these boundary conditions along with (3.15), (3.16), and (3.19) to solve for the homogenous solution coefficients, we find (Appendix A.2.2) that the solution for $\widehat{\rho}$ is [Fourcaud and Brunel, 2002]

$$\widehat{\rho} = \frac{r_0}{i\omega}[e^{u-u_\theta} - \Theta(u_r - u)(e^{u-ur}) - e^{z_+(\omega)(u-u_\theta)} + \Theta(u_r - u)e^{z_+(\omega)(u-u_r)}] \tag{3.35}$$

and the solution for the firing rate modulations $\widehat{n}(\omega)$ is

$$\widehat{n}(\omega) = \frac{\sqrt{1 + 4i\omega\tau_e} - 1}{2i\omega\tau_e}. \tag{3.36}$$

3.2.1 Gain and Phase of the Response

Figure 3.2 shows that for perturbations in the variance, the PIF acts like a high-pass filter. The response grows as $\sqrt{\frac{1}{\omega\tau_e}}$ for high frequencies. The response

is synchronous for high frequencies, showing little phase shift. However, for lower frequencies, the phase shift goes to 90°. Notice that as μ_0 increases, τ_e decreases, and therefore the overall gain curve is attenuated.

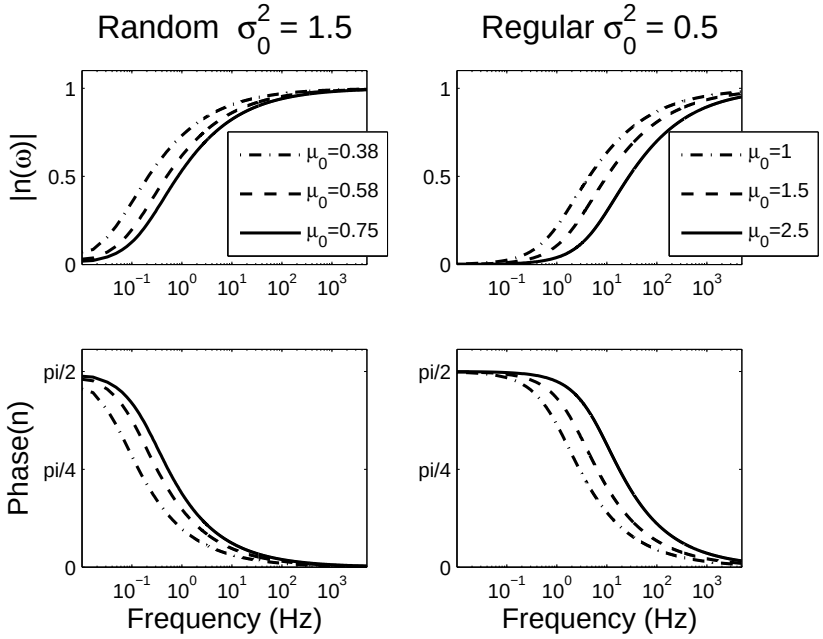

Figure 3.2: Gain and phase curves for the PIF model due to perturbations in the variance. The PIF model acts like a high-pass filter independent of regime. Phase shifts are 90° in the low-frequency limit and go to zero in the high-frequency limit.

Figure 3.3 shows that when μ is perturbed, the PIF acts like a low-pass filter. The response is synchronous for low-frequency perturbations in the mean, showing little phase shift. As the perturbation frequency increases, the phase shift becomes larger eventually reaching values of $-45°$. For mean perturbations, increasing τ_e increases the overall gain of the model. Letting $\omega = \frac{1}{\tau_e}$, the gain is equal to 0.69 for all τ_e. Therefore, $\frac{1}{\tau_e}$ acts as a natural cutoff frequency for the gain due to mean perturbations.

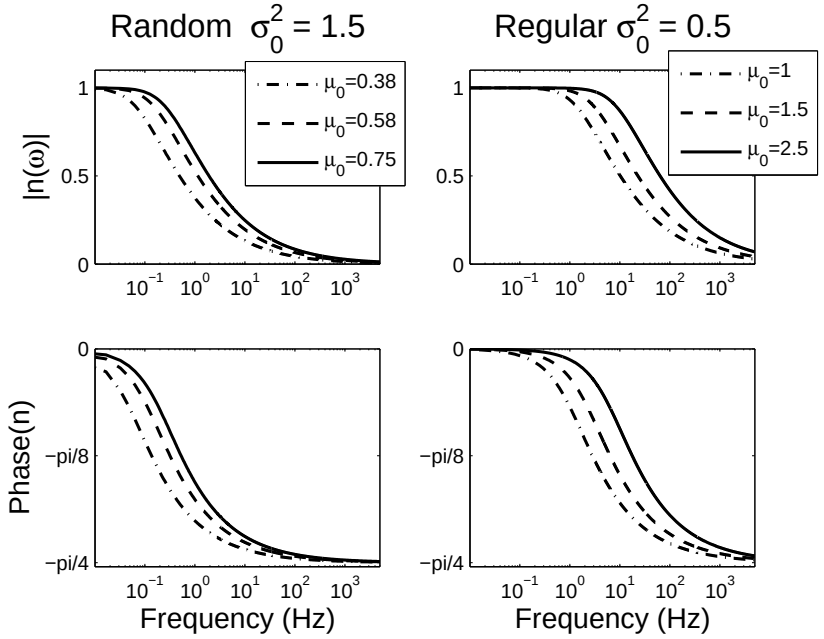

Figure 3.3: Gain and phase curves for the PIF model due to perturbations in the mean. The PIF model acts like a low-pass filter independent of regime. Phase shifts are zero in the low-frequency limit and go to $-45°$ in the high-frequency limit.

3.3 Perturbations in Both Parameters Concurrently

Assuming inputs are Poisson, the mean and the variance of the pre-synaptic input rate, $\lambda(t)$, are equal. Once we move to the diffusion approximation, the mean and variance of the input are proportional, $\mu(t) = \overline{Q}\lambda(t)$ and $\sigma^2(t) = \overline{Q}^2\lambda(t)$ (see chapter 2). Therefore changes in the pre-synaptic input rate would cause proportional changes in the mean and variance of the input. For mean and variance perturbations, ϵ is used equivalently since μ_0 and σ_0^2 are factored out (see equations (3.3) and (3.26). Since we expect proportional changes in the rate for Poisson inputs, the 1st order response is then the sum of the 1st order responses to the parameters varied separately.

Upon closer examination of equations (3.25) and (3.36), we see that the response to perturbations in the variance is 1 minus the response to perturbations in the mean. Summing these two quantities gives a gain of 1 at all frequencies. Thus, the population firing rate response of the PIF is a scaled replica of the input rate signal for Poisson distributed inputs.

3.4 Discussion

Previous work by Fourcaud and Brunel showed that by sinusoidally perturbing the mean of the synaptic input, the PIF in FP form acted like a low-pass filter. However, Knight has previously shown that the PIF acted like a perfect replicator of sinusoidal signals to deterministic input. In this chapter, we have shown that when the variance of the input is sinusoidally perturbed, the PIF response is the

compliment of the response to mean perturbations, acting like a high-pass filter.

Considering both excitatory and inhibitory input rates, we can independently alter the total mean and variance of the current. In the simplest case, if we hold the total input rate constant, while varying the ratio of excitatory to inhibitory input, the mean of the current will change. Alternatively, if we change the total rate of input, while keeping the ratio of excitatory to inhibitory input the same, the variance will change. The PIF responds oppositely to changes in the mean versus the variance, low-pass versus high-pass respectively. Neurons may utilize the different input parameters to encode signals of different speeds.

In this chapter, we have shown that PIF in FP form can respond like an all-pass synchronous filter by considering simultaneous perturbations in the mean and the variance of the synaptic input. Since input is frequently modeled as Poisson, it makes sense to alter the mean and the variance of our Gaussian approximated white noise process together and by the same amount. Therefore symmetric with the deterministic case, we have shown that the response of a population of PIF neurons will exactly replicate a stochastic signal.

The response due to perturbations in either parameters is dependent on the time constant τ_e, which is the ratio of the variance of the signal to two times the squared mean. For mean perturbations, $\frac{1}{\tau_e}$ acts as a natural cutoff frequency for the low-pass filtering. Future work will focus on studying the relationship between this new time constant and the response of more realistic models.

Chapter 4

Response Dynamics of the LIF Model

4.1 Introduction

The leaky integrate-and-fire (LIF) model is the simplest neuron model that captures the essential properties of neuronal signaling: integration of inputs by a capacitive cell membrane, a voltage threshold leading to the generation of a stereotyped action potential, and a subsequent re-polarization of the membrane. Because of its simplicity and analytic tractability, the LIF has been used as the basic building block in models of large networks [Hansel and van Vreeswijk, 2002, Koene and Hasselmo, 2005, Hasselmo, 2005, Barak and Tsodyks, 2006] as well as to investigate fundamental properties of neuronal spiking behavior [Tuckwell, 1988, Burkitt, 2006b, Burkitt, 2006a]. Yet basic properties of LIF dynamics remain poorly understood. For example, a common intuition is that the low-pass filtering of the membrane voltage should carry over to firing rate dynamics [Wilson and Cowan, 1973]. However, it has been shown that the response time of simple model neurons can be much faster than the membrane time constant [Holt et al., 1997, Silberberg et al., 2004], and that the LIF can display complex resonance effects [Gammaitoni et al., 1998, Plesser and Geisel, 1999, Plesser and Gerstner, 2000, Plesser and Geisel, 2001]. Lacking a deeper understanding of the LIF model, it can be difficult to determine if the dynamics of more realistic neuron models stem from greater biological detail, or

follow directly from the basic dynamics of integrate, fire, and reset.

One complication in understanding LIF dynamics is that the same LIF model can operate in two qualitatively distinct regimes of behavior, depending on the input [Abeles, 1991, Troyer and Miller, 1997]. If the mean input current is large and synaptic noise is small, the model operates in the Regular Regime. Voltage is driven monotonically across spike threshold, and spikes are produced at regular intervals determined mostly by the mean input [Salinas and Sejnowski, 2002]. In this regime, the model acts like an oscillator and, like many oscillators, displays resonant behavior for input modulations near its baseline firing frequency [Knight, 1972a]. If the mean input is subthreshold but the noise is large, the model operates in the Random Regime. Voltage trajectories follow a random walk with occasional threshold crossings and spike times are irregular [Gerstein and Mandelbrot, 1964, Shadlen and Newsome, 1994]. Since the probability of producing a spike depends on the amplitude of noise fluctuations as well as the mean input, it is possible to transmit signals by changing the input variance. It has been shown that LIF-like models respond more rapidly to changes in the variance than to the mean of the input current [Lindner and Schimansky-Geier, 2001], and this rapid response has been confirmed in real neurons [Silberberg et al., 2004].

Although many aspects of LIF dynamics have been illustrated in previous studies e.g. [Brunel et al., 2001, Fourcaud and Brunel, 2002, Fourcaud-Trocmé et al., 2003, Lindner and Schimansky-Geier, 2001, Naundorf et al., 2005], these results are often presented in the context of other specific research questions. To obtain a coherent picture of the full range of LIF behavior, we systematically studied the response

dynamics of LIF neurons driven by stochastic inputs. We consider input signals carried by changes in both the variance and mean of the input current, and choose baseline parameters that cover the range of LIF behavior. Exploiting the simplicity of the LIF model and using methods from stochastic differential equations, we reduce the analysis to a consideration of the probability density as a function of voltage and time [Brunel and Hakim, 1999, Knight, 2000, Fourcaud and Brunel, 2002, Silberberg et al., 2004]. We then characterize model output using the ensemble firing rate, the instantaneous probability of crossing threshold and producing a spike, calculated over an ensemble of neurons subject to input with the same noise statistics.

To facilitate the comparison across input signals and regimes of behavior, and as a first step to understanding the full non-linear response of the LIF, we focus on characterizing the linear response to sinusoidal modulations of the mean and variance of the input current. We find that low pass membrane filtering dominates the response dynamics for changes in the mean current, but that modulations in the variance can lead to qualitatively different response properties depending on the regime of model behavior. We argue that the differences between modulating the variance versus the mean of the input current can be understood by noting that the analytic expression for the ensemble firing rate decomposes into the product of two terms: the first term captures the fast noise jitter, which depends exclusively on the input variance; the second term is dependent on the integrative properties of the membrane and involves both the mean and the variance of the input.

4.2 Methods

We investigate the response dynamics of the leaky integrate-and-fire model (LIF):

$$C\frac{dV}{dt} = g_L(V_L - V) + I(t), \tag{4.1}$$

where V is the membrane voltage, $I(t)$ is the time-varying stochastic input current, the membrane time constant $\tau(= \frac{C}{g_L})$ is set to 10 $msec$, $C(= 1\mu F/cm^2)$ is the membrane capacitance, $g_L(= 0.1mS/cm^2)$ is the leak conductance, and $V_L(= -70mV)$ is the reversal potential of the leak channels. The neuron spikes when the voltage reaches a threshold voltage ($\theta = -60mV$), after which the voltage is reset ($V_r = -70mV$). For simplicity, we did not include an absolute refractory period. Adding a fixed refractory period does little to the dynamics other than slow the mean firing rate and push the model further toward regular spiking behavior. Furthermore, an LIF model with a relatively strong after-spike reset but short refractory period has similar behavior as a model with a longer refractory period but weaker reset.

4.2.1 Stochastic Differential Equation

Since spiking in real neurons is noisy, the synaptic current $I(t)$ is commonly modeled as stochastic (see chapter 2. If individual synaptic inputs are instantaneous, weak, and uncorrelated in time, we can adopt a diffusion approximation in which the input current $I(t)$ is decomposed into the mean current $\mu(t)$ plus fluctuations $\sigma(t)\eta(t)$, where $\eta(t)$ is a Gaussian white noise process [Brunel and Hakim, 1999,

Knight, 2000, Fourcaud and Brunel, 2002, Silberberg et al., 2004]. $\mu(t)$ represents the mean charge accumulating per time and has units $nC/(cm^2 msec) = \mu A/cm^2$. $\sigma^2(t)$ measures the variance of the charge accumulating per time and has units $nC^2/(cm^4 msec) = \mu A^2 msec/cm^4$.

We use the Fokker-Planck (forward Kolmogorov) approach [Ricciardi, 1977, Brunel and Hakim, 1999, Fourcaud and Brunel, 2002, Allen, 2003] to track the probability density function over voltage, $\rho(V,t)$, as it changes in response to modulations in the input. $\rho(V,t)$ represents the probability that a given trajectory is near the voltage V at time t. For any given voltage the net flux or "rate of flow" $J_V(V,t)$ across that voltage can be calculated as:

$$J_V(V,t) = -\frac{R^2\sigma^2(t)}{2\tau_m^2}\frac{\partial\rho(V,t)}{\partial V} + \frac{(V_L - V(t)) + R\mu(t)}{\tau_m}\rho(V,t) \tag{4.2}$$

The probability density obeys the following dynamics:

$$\tau_m\frac{\partial\rho(V,t)}{\partial t} = \tau_m\ \frac{-\partial J_V(V,t)}{\partial V} \tag{4.3}$$

$$= \frac{R^2\sigma^2(t)}{2\tau_m}\frac{\partial^2\rho(V,t)}{\partial V^2} - \frac{\partial}{\partial V}[(V_L - V(t)) + R\mu(t)]\rho(V,t). \tag{4.4}$$

Boundary conditions are needed to account for spike threshold and voltage reset. Threshold is modeled as an absorbing boundary imposed at a voltage θ, and the firing rate is simply the flux crossing threshold, $r(t) = J_V(\theta,t)$. This probability flux is then re-injected at voltage reset [Brunel and Hakim, 1999, Brunel, 2000, Fourcaud and Brunel, 2002]. Under the standard diffusion approximation, the density must be equal to zero at an absorbing boundary, so the firing rate equation becomes

$$r(t) = J_V(\theta,t) = \frac{R^2\sigma^2(t)}{2\tau_m^2}\left(-\frac{\partial\rho}{\partial V}(\theta,t)\right). \tag{4.5}$$

Note that the firing rate equation is a product of two terms. Since the density goes to zero at threshold, the second term is proportional to the area under the probability density function near threshold. We interpret this term as indicating the probability that the voltage lies within a small boundary layer near threshold and denote it $B(t) = -\partial\rho/\partial V(\theta, t)$. The first term is proportional to the instantaneous level of input variance. Thus, the firing rate is equal to the probability that a trajectory lies near threshold multiplied by the probability that the trajectory will "jump" across threshold. The multiplicative constitution of the firing rate equation is key in understanding the nature of the dynamic response of the LIF model to changing inputs. Numerical simulations were performed using MATLAB (Mathworks, Natick, MA) For a description of the numerical simulations see chapter 2.

4.3 Linear Systems Analysis

To compare IF dynamics across the regimes of model behavior, we took a linear systems approach, measuring the gain and phase of the response to sinusoidal perturbations in the input parameters $\mu(t)$ and $\sigma^2(t)$. We will use the subscript '0' to denote the baseline value of the parameter (the '0th' harmonic), and the subscript '1' to denote the amplitude of the sinusoidal modulation (the 1st harmonic), except in chapter 3 where the normalized 1st harmonic of the response is denoted $\widehat{n}(\omega)$ following Fourcaud and Brunel's notation [Fourcaud and Brunel, 2002].

To measure the gain and the phase of the response, we performed a Fourier decomposition of the firing rate $r(t)$ and found the dominant component of the

response modulation $r_1(\omega)\cos(\omega t+\phi)$. Since the baseline firing rate r_0 varies widely over the range of parameters μ_0 and σ_0^2, we characterized the response gain as the fractional change in firing rate from baseline, $r_1(\omega)/r_0$, divided by the fractional change in the input, μ_1/μ_0 or σ_1^2/σ_0^2:

$$G_\mu(\omega) = \frac{r_1(\omega)/r_0}{\mu_1/\mu_0}, \tag{4.6}$$

$$G_{\sigma^2}(\omega) = \frac{r_1(\omega)/r_0}{\sigma_1^2/\sigma_0^2}. \tag{4.7}$$

The response phase ϕ was calculated as the difference between the phase of the input and response. Phase lags were assigned negative values and phase advances positive values.

Since larger input perturbations can result in non-linear firing rate responses of integrate-and-fire type models [Pressley and Troyer, 2006], we set input modulations sufficiently small to stay within the linear regime of response, (μ_1 to 0.0625 $\mu A/cm^2$ and of σ_1^2 to 0.0625 $\mu A^2 msec/cm^4$; $> 95\%$ of response power at the input modulation frequency).

The LIF acts like a low-pass filter to mean perturbations. The cutoff frequency of the filter is calculated as the frequency at which the gain is reduced to $\frac{1}{\sqrt{2}}$ times the the low-frequency gain.

4.4 Results

4.4.1 Range of Model Response

The two basic regimes of model behavior are illustrated in figure 4.1. In the Random Regime, the membrane voltage follows a random walk below threshold (top left). The distribution of voltages has a near Gaussian shape, with only slight distortions due to the occasional spiking and reset (bottom left). In the Regular Regime, the voltage is driven to suprathreshold levels and spiking is nearly oscillatory (top right). The distribution of voltages is almost entirely confined between reset and spike thresholds (bottom right). More probability is near threshold because the voltage trajectories are slowed due to increases in the leak current as the membrane is depolarized.

To illustrate the wide range of response dynamics that can be displayed by a single LIF model, we simulated the effect of step-like increases in the mean and variance of the input. The pre-step levels of the mean and variance (μ_0 and σ_0^2 respectively) were set so that the model was operating in the two basic regimes of behavior (Fig. 4.2). In the left column, input levels are such that the model shows Random Regime behavior ($\mu_0 = 0.25\ \mu A/cm^2$ and $\sigma_0^2 = 1.5\ \mu A^2 msec/cm^4$); in the right column the model operates in the Regular Regime ($\mu_0 = 1.5\ \mu A/cm^2$ and $\sigma_0^2 = 0.5\ \mu A^2 msec/cm^4$). The top row shows the response to changes in the mean current with the noise held fixed ($\Delta\mu/\mu_0 = 20\%$); the bottom row shows the response to changes in the input variance ($\Delta\sigma^2/\sigma_0^2 = 20\%$).

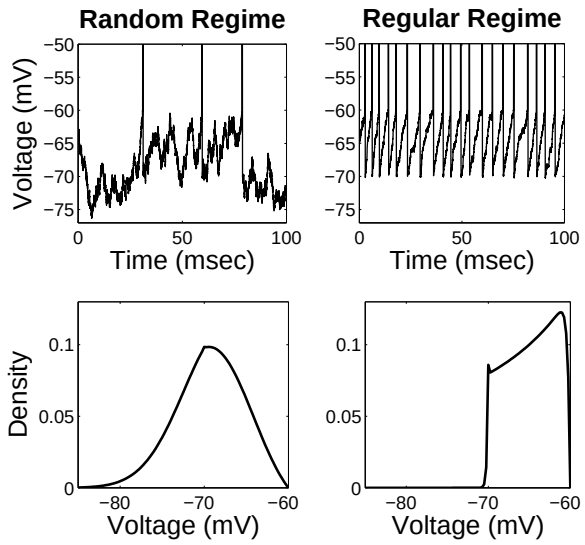

Figure 4.1: Two regimes of behavior. Top: typical voltage traces. Left: Random Regime; Right: Regular Regime. Bottom: typical probability density functions in the two regimes.

4.4.2 Perturbations of the Mean

A common intuition is that the capacitive filtering of the membrane voltage should carry over to firing rate dynamics, an intuition that is largely correct for perturbations in the mean (but see Fig. 4.3; [Brunel et al., 2001]). As can be seen in figure 4.3, the gain of the response is low-pass, roughly constant for low frequencies and then decaying toward zero at higher frequencies.

However, when the the model is in the Regular Regime, the cutoff frequency is systematically related to the steady-state firing rate (4.4 top right. Here the cutoff frequency is measured as the frequency at which the gain is reduced to $\frac{1}{\sqrt{2}}$ times the low-frequency gain. Figure 4.3 also shows the phase of responses in both the Regular and Random Regime. These will be discussed after the presentation of the

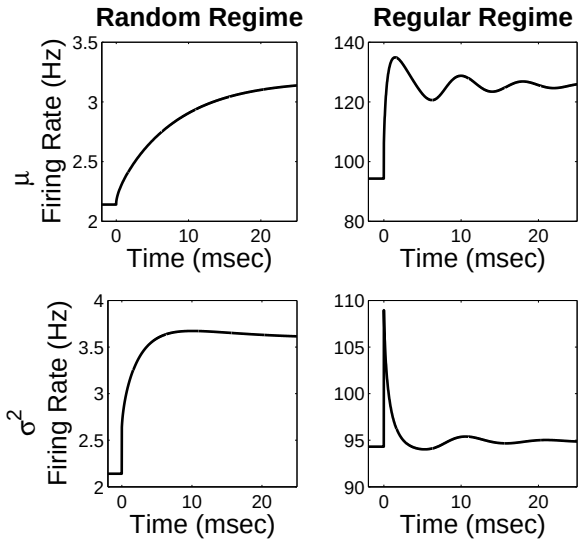

Figure 4.2: Response to step changes in input parameters at time = 0 msec. Top: increases in the mean input. Bottom: increases in input variance. Left: Random Regime; Right: Regular Regime. Firing rate dynamics depend strongly on the regime of LIF behavior and on which parameter is increased.

phase response for variance modulations.

An additional property of LIF response dynamics to perturbations in the mean is the existence of resonances in the response. Early work by Knight [Knight, 1972a, Knight, 1972b] revealed amplifications of the response when the mean of the input is modulated at a frequency equal to the underlying firing rate of the neuron (the firing rate when the mean and variance are constant in time). Such resonances are commonly seen in oscillatory systems when driven at their natural frequency. Accordingly, the resonances found for modulations of the mean occur in the Regular Regime, where the firing is nearly oscillatory (figure 4.3). In the Random Regime, where firing is unpredictable and the mean input is subthreshold, resonances are not found.

4.4.3 Perturbations of the Variance

The LIF model responds quite differently to modulations in the variance than it does to modulations in the mean input current (Fig. 4.5). Perhaps the most striking difference is the large gain at high frequencies [Lindner and Schimansky-Geier, 2001]. The underlying reason for large high-frequency gain becomes clear if one examines the multiplicative nature of the firing rate (equation (4.5)). The firing rate $r(t)$ is proportional to the instantaneous variance, $\sigma^2(t)$, times the probability lying within a boundary layer just below threshold, $B(t)$ (see Methods). For very high-frequency modulations, the integrative nature of membrane dynamics limits shifts in the voltage distribution, causing $B(t)$ to remain essentially constant. Therefore, in the

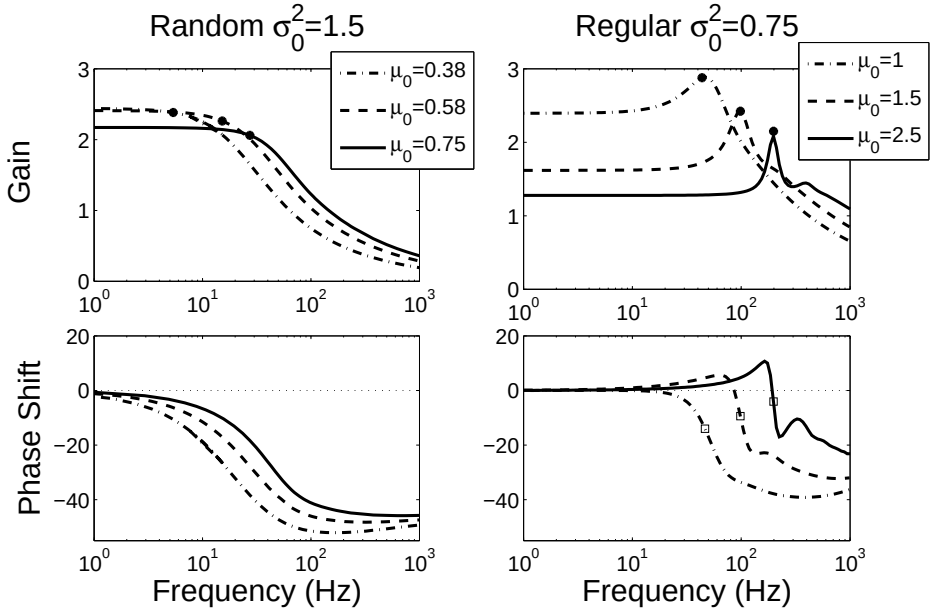

Figure 4.3: LIF response to perturbation in the mean. Top: gain; Bottom: phase. Left: Random Regime; Right: Regular Regime. The gain is constant at low frequencies and decays to zero in the high-frequency limit. Black dots show the steady-state firing frequency. The phase shift goes to $-45°$ in the high-frequency limit [Brunel et al., 2001]. Squares on the phase curves mark the peak frequency of the resonance in the gain curve.

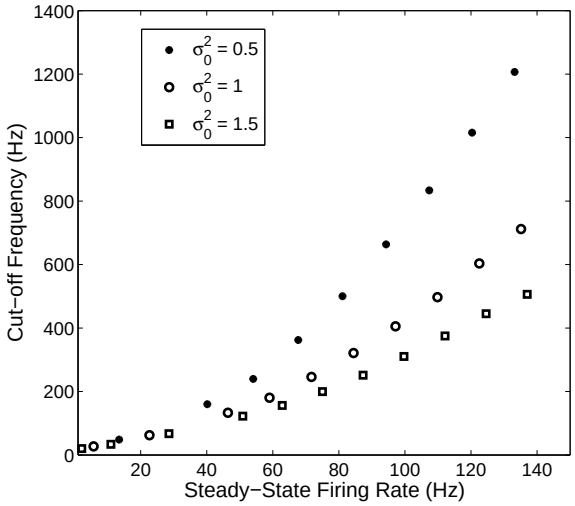

Figure 4.4: Cutoff frequency is systematically related to steady-state firing rate. Cutoff frequencies are plotted against steady-state firing rate for variance levels of $0.5\mu A^2 msec/cm^4$, $1\mu A^2 msec/cm^4$ and for $1.5\mu A^2 msec/cm^4$.

high-frequency limit, the firing rate is proportional to the instantaneous variance, $\sigma^2(t)$. Proportionality implies that a fractional change in the variance leads to the same fractional change in firing rate. It follows that

$$\lim_{\omega \to \infty} G_{\sigma^2}(\omega) = 1. \tag{4.8}$$

Figure 4.5 also shows that the gain increases toward 1 at high frequencies in the Regular Regime and decreases toward 1 in the Random Regime. The boundary between the two happens when $\mu_0 > 1\mu A/cm^2$, ie when the mean input is just sufficient to depolarize the cell to threshold (fig. 4.5 top). Thus the division between increasing or decreasing gain for high frequencies corresponds to a common dividing line between the Random and Regular Regimes of LIF behavior [Bulsara et al., 1996].

At very low frequencies, we can assume that the firing rate can be approxi-

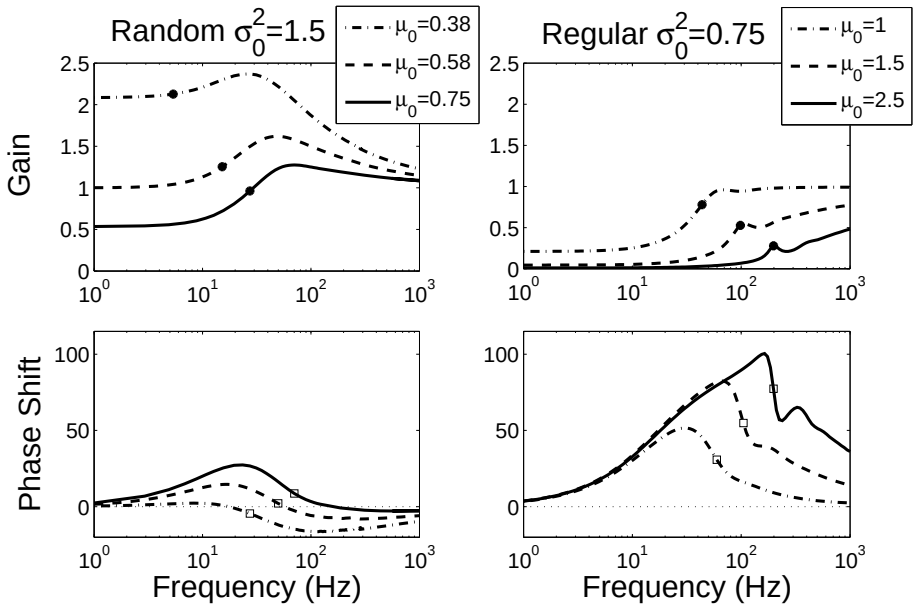

Figure 4.5: LIF response to perturbation in the input variance. Panels and markings same as fig. 4.3. In both regimes, the gain stays finite at high frequencies, and the phase goes to zero at both low and high frequencies. At low frequencies, response gain goes to zero in the Regular Regime ("high-pass" behavior), but stays large in the Random Regime ("all-pass" behavior).

mated by the steady-state behavior for the current value of the input. Let $\tilde{r}(\sigma^2)$ denote the steady-state firing rate for input with constant variance σ^2. (The mean input is assumed fixed at μ_0.) Then for small and slow changes in the variance

$$r(t) = \tilde{r}\left(\sigma_0^2 + \sigma_1^2 \cos(\omega t)\right) = \tilde{r}\left(\sigma_0^2\right) + \sigma_1^2 \cos(\omega t)\ \frac{\partial \tilde{r}}{\partial \sigma^2}(\sigma_0^2) \tag{4.9}$$

and

$$\lim_{\omega \to 0} G(\omega) = \frac{r_1/r_0}{\sigma_1^2/\sigma_0^2} = \frac{\left(\sigma_1^2 \partial \tilde{r}/\partial \sigma^2\right) / \left(\tilde{r}(\sigma_0^2)\right)}{\sigma_1^2/\sigma_0^2} = \frac{\partial \tilde{r}}{\partial \sigma^2}(\sigma_0^2)\ \frac{\sigma_0^2}{\tilde{r}(\sigma_0^2)}. \tag{4.10}$$

Therefore, the gain will be proportional to $\partial \tilde{r}/\partial \sigma^2$, the derivative of the steady-state firing rate as a function of the variance. In the Regular Regime, changing the variance has little effect on the firing rate since the mean return time to threshold depends mostly on mean input current [Salinas and Sejnowski, 2002]. Thus, $\partial \tilde{r}/\partial \sigma^2$ is small and the gain is near zero (Fig. 4.5, top right). In the Random Regime, increasing the variance leads to a significant increase in the probability of a random crossing threshold event, and the low-frequency gain is finite (Fig. 4.5, top left).

To further understand the low-frequency gain, we again exploit the multiplicative decomposition of the firing rate. We write $\tilde{r}(\sigma^2) = (R^2\sigma^2/2\tau_m^2)\tilde{B}(\sigma^2)$, where the second term is the boundary layer term at equilibrium for input with variance σ^2. Then

$$\frac{\partial \tilde{r}}{\partial \sigma^2}(\sigma_0^2) = \frac{R^2 \tilde{B}(\sigma_0^2)}{2\tau_m^2} + \frac{R^2\sigma_0^2}{2\tau_m^2}\ \frac{\partial \tilde{B}}{\partial \sigma^2}(\sigma_0^2) \tag{4.11}$$

$$\lim_{\omega \to 0} G_{\sigma^2}(\omega) = 1 + \frac{R^2\sigma_0^4}{2\tau_m^2 \tilde{r}(\sigma_0^2)}\ \frac{\partial \tilde{B}}{\partial \sigma^2}(\sigma_0^2). \tag{4.12}$$

Since the high-frequency gain is equal to 1, we conclude that the low-frequency gain is larger than the high-frequency gain when $\partial \tilde{B}/\partial \sigma^2 > 0$ and vice versa.

To interpret this result, first consider a model operating in the Regular Regime. The drift toward threshold dominates the dynamics, and as long as the model stays in the Regular Regime, changing the variance will have little effect on the steady flow of trajectories entering the subthreshold boundary layer. However, increasing the variance *does* cause individual trajectories to cross threshold and leave the subthreshold boundary layer with greater probability, i.e. it increases $R^2\sigma^2(t)/(2\tau_m^2)$. Since changing the variance does not change the overall firing rate, it must be the case that increasing the variance causes a decrease in the number of trajectories within the boundary layer, i.e. $\partial\tilde{B}/\partial\sigma^2 < 0$.

Now consider a model operating in the Random Regime. The mean input is significantly below threshold and spikes occur only for fluctuations into the tails of the voltage distribution (eg fig. 4.1, bottom left). An increase in input variance will immediately increase the firing rate by increasing the probability of jumping from the boundary layer across threshold, but will also eventually lead to a broadening of the voltage distribution. If the model is far into the Random Regime, the broadening of the distribution will lead to a greater number of trajectories remaining the in the boundary layer below threshold, even in the face of greater rate of jumping across threshold. This net increase in the density within the boundary layer can be written as $\partial\tilde{B}/\partial\sigma^2 > 0$, and indicates that subthreshold random behavior has become dominant relative to the effects of spiking and reset.

The parameter dependence of the high and low-frequency gain in response to modulations in the variance are summarized in figure 4.6. The contour lines indicate level curves of the low-frequency gain, and darker gray indicates parameters where

this frequency gain exceed the high-frequency gain (ie low-frequency gain > 1). For these parameters, $\partial \tilde{B}/\partial \sigma^2 > 0$ and Random Regime behavior dominates. We propose that parameters in the white area between these extremes should be considered as an intermediate regime between Regular and Random spiking behavior. The light gray area shows parameter values ($R\mu_0 > 10\ mV$) leading to high-frequency gains that approach the limiting value of 1 from below (Fig. 4.5, top right). These values are in the Regular Regime.

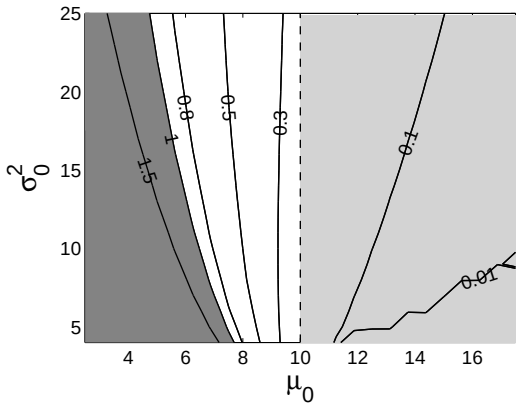

Figure 4.6: Contour plot of low-frequency gain due to variance modulations. Region where gain is greater than 1 is the Random Regime, where LIF acts like an all-pass filter (dark grey). Region where $R\mu_0 > 10\ mV$ (suprathreshold mean input) is the Regular Regime, where the low-frequency gain is small and the LIF acts like a high-pass filter (light grey). White region signifies an Intermediate Regime.

4.4.3.1 Resonances

Perturbations in the variance lead to resonances, in which response gain is amplified over a specific range of frequencies [Lindner and Schimansky-Geier, 2001]. These resonances differ significantly from the those caused by modulating the mean input current. For the mean, the resonances are found only in the Regular Regime and the peak of the resonance closely tracks the oscillation frequency of the underlying system (i.e. the firing rate) at steady-state (Figs. 4.3 and 4.7, solid line). For the variance, the peak frequency of the resonance in the Regular Regime is consistently higher than the mean oscillation frequency, with this difference increasing as one moves more toward Random Regime behavior (Fig. 4.7, dashed line). Furthermore, modulating the variance also leads to resonances in the Random Regime, a phenomenon that is completely absent for modulations of the mean, and the mean oscillation frequency is outside of the resonance band.

4.4.4 Phase Response

Although we have focused on the gain, a complete characterization of linear response properties requires a specification of the phase lead or lag at each frequency. The firing rate responses of LIF neurons to modulations in the mean are consistent with those of a leaky integrator (fig. 4.3C): at low frequencies the input changes much more slowly than the membrane time constant and so the response follows the signal with near zero phase difference; at higher frequencies, the process of integration takes time to build up, leading to a phase lag (negative difference)

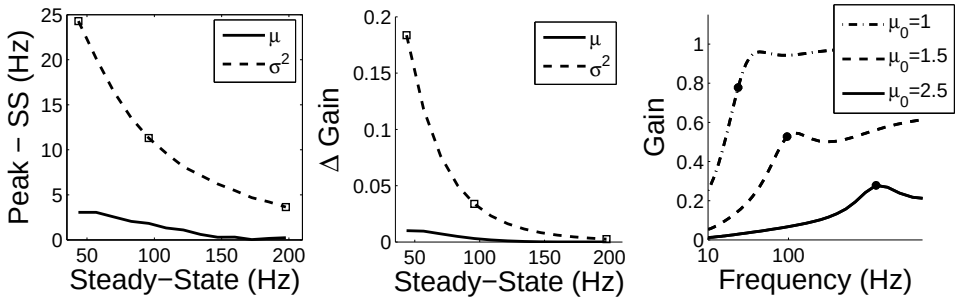

Figure 4.7: Left panel: Frequency difference between peak resonance frequency and steady-state firing rate in the Regular Regime. σ_0^2 was held fixed at $0.75\mu A^2 msec/cm^4$. μ_0 ranged from $1 - 2.5\mu A/cm^2$, leading to firing rates ranging from 43-197 Hz. Middle panel: Difference in gain for response due to peak resonance frequency and steady-state firing rate in the Regular Regime, same parameters as in left panel. Right panel: gain curves for variance modulation at the points marked with a square (μ_0 = 1, 1.5 and 2.5 $\mu A/cm^2$), with the steady-state firing rate marked *.

between signal and response. In the Regular Regime, the overall trend is the same, but with additional phase shifts near the resonance frequency (fig. 4.3D). For input frequencies slightly slower than the resonance frequency, the system tends to "speed up" the output, leading to more positive phase differences. For inputs slightly faster than the resonance frequency, the system response is "slowed down" leading to more negative phase differences.

For variance modulations in the Random Regime, the phase response is dominated by a transition from positive to more negative phase shifts, with the transition occurring near the peak of the broad resonance found in this regime (fig. 4.5C, squares). Consistent with gain curves that pass all frequencies, phase shifts are small overall. Parameters leading to more low-pass gain curves have more negative phase shifts and those leading to more high-pass behavior have more positive phase shifts.

In the Regular Regime, phase responses have an overall positive shift consistent with high-pass behavior (fig. 4.5D). However, a prominent positive peak in the phase curve is seen at intermediate to high frequencies, with smaller phase shifts at higher frequencies. On top of this overall trend, additional positive and negative phase shifts surround the resonance peaks.

4.5 Discussion

This chapter considers how the parameters of time-varying stochastic synaptic input affect the response dynamics of the leaky integrate-and-fire model. Two fea-

tures of the input were varied: the baseline input parameter values, which determine the underlying response regime, and the parameter used to encode the signal, either the mean or the variance of the input. Other researchers have provided results that account for a subset of possible combinations of these parameters. In this work, we surveyed the response dynamics to changes in both the mean and the variance of the input over a wide range of baseline input parameters to develop a comprehensive picture of LIF dynamics. We found that LIF response differed depending not only on which parameter encoded the signal but also the underlying regime of behavior.

Lindner and Schimansky-Geier [Lindner and Schimansky-Geier, 2001] investigated LIF response when the signal was encoded in both the mean and the variance of the input and then analyzed the response components separately. However, their focus was determining if stochastic resonances appeared for both encoding parameters, and since stochastic resonance occurs for weak (subthreshold) signals, their analysis only included Random Regime baseline parameters. They found that stochastic resonances occurred for both encoding parameters and that the overall peak response to the noise-encoded signal occurred at a finite frequency. Additionally, they determined that LIF response was finite for arbitrarily fast signals, if the signal was encoded in the variance. Their figures show the all-pass behavior of the LIF to variance encoded signals in the Random Regime and the Random Regime resonances, that we analyze and confirm in this work. We have extended their results by analyzing LIF response to noise-encoded signals in the Regular Regime. We find that in the Regular Regime, LIF response is still finite to arbitrarily fast signal changes, when the signal is encoded in the variance, however, the model acts like a

high-pass filter, with the low-frequency gain nearly zero for very Regular baseline parameters.

The low-frequency response can be used to develop a taxonomy of response regimes, with a higher low-frequency gain to noise-encoded signals suggesting Random Regime behavior and near zero low-frequency gain suggesting Regular Regime behavior, with threshold mean input acting as a loose boundary between regimes. Our analysis of the noise-encoded signals in the Random Regime shows that increasing the noise amplitude increases the spread of the pdf, causing a larger amount of trajectories in the boundary layer near threshold, even as more are jumping across. The increased number of trajectories in the threshold boundary layer causes the finite low-frequency gain in the Random Regime. Further analysis shows that not only does the LIF act all-pass, but low-frequency response can be higher than the high-frequency responses. We have shown that in the Regular Regime, the increase in noise amplitude decreases the amount of trajectories in the boundary layer, causing a decreasing low-frequency response as we move farther into the Regular Regime.

For perturbations in the mean, Brunel and colleagues studied LIF response for baseline input parameters that accounted for both regimes of neuron behavior [Brunel et al., 2001, Fourcaud and Brunel, 2002]. They showed that the LIF acts like a low-pass filter to mean-encoded signals and that the gain decays as $\frac{1}{\sqrt{\omega}}$ after a cutoff frequency, with the phase of response shifting as much as $-45°$. Here we show that the cutoff frequency is systematically related to the steady-state firing rate. And in the Regular Regime, the model responds faster than expected from filtering due to the membrane time constant. Additionally, Brunel confirmed Knights results

[Knight, 1972a] that for perturbation frequencies that are multiples of the steady-state firing rate, resonances exist in the gain and these resonances decrease as the baseline noise increases.

For noise-encoded signals, we also found resonances in the gain of the response. Unexpectedly, these resonances peak at frequencies greater than the steady-state firing rate. The difference of the peak of the resonance from the steady-state firing rate increases as the baseline parameters become less "Regular", with lower mean rates and higher noise. This difference suggests the mechanism for generating resonances for noise-encoded signals is is different from the that which causes resonances for mean-encoded signals. We hypothesize that there are two mechanisms, one that cause the resonances seen in the Random Regime for noise-encoded signals, and the usual mechanism first described by Knight that causes resonances for mean-encoded signals. We speculate that both of these mechanisms combine to create the resonances in the Regular Regime for variance-encoded signals.

Our overall analysis suggests that the differences in LIF response emanate from the product of two terms in the firing rate equation, the first term is a weighted version of the input variance and the second term is proportional to the amount of probability in a boundary layer near threshold and is altered more slowly as the mean and variance perturbations change the shape of the pdf.

Chapter 5

The Effect of Synaptic Dynamics on LIF Response

5.1 Introduction

In this chapter, we investigate how the inclusion of synaptic dynamics affects the response of the LIF model. We assume that neurotransmitter accumulates on receptors much faster than it becomes unbound, and approximate synaptic currents with an instantaneous rise and slower decay [Destexhe et al., 1998]. The unbinding time course differs based on receptor type and typically falls in the range of 2-100 msec [Destexhe et al., 1998]. As a simplifying approximation, we ignore the rise time of the current, which is caused by the time length of release of neurotransmitter from the pre-synaptic neuron. Ignoring the rise time is feasible since it is much shorter than the unbinding time.

We ask two questions about this model. First, how does the response to this more realistic model (the 2D model), compare with the response of the LIF when the input is modeled as having an instantaneous time course (the 1D model)? Second, is the response to the 1D model, the limiting response of the 2D model, if we let the decay time go to zero? To address these questions, we draw two comparisons. The linear response dynamics of the 2D equation are governed by two linear filters, one that takes pre-synaptic rates to current, and the other that takes current to firing rate. The first comparison we draw is between the linear response of the 1D model

to the linear response of the 2D model, considering the total transformation which is also a linear filter that accounts for the full transformation from input rates to output rates. But since the first transformation is a low-pass filter, which causes the full transfer function to act as a low-pass filter, we factor out the first transformation to see if synaptic dynamics affect the voltage response, based on something other than the low-pass filtering of the current.

As in the previous chapter, we survey the response over the qualitatively different regimes of behavior, as well as for both mean and variance encoding. We note that the firing rate equation of the 2D model is a product of two terms, one that includes the current term, and the other which delineates the amount of trajectories near threshold.

5.2 Setting Parameters for Comparison

The main goal of this chapter is to compare the linear response dynamics of the LIF model with white noise currents:

$$\tau_m \frac{dV}{dt} = -V + V_L + R\overline{Q}S(t) \tag{5.1}$$

to the response dynamics of the LIF model with finite synaptic dynamics:

$$\tau_m \frac{dV}{dt} = -V + V_L + RI_s(t) \tag{5.2}$$

$$\tau_s \frac{dI_s}{dt} = -I_s + \overline{Q}S(t), \tag{5.3}$$

where we often approximate the input spike train $S(t)$ as a white noise process $S(t) = \mu_s(t) + \sigma_s(t)\eta(t)$ (see Methods). Since synaptic dynamics lead to a two-

dimensional state space, we refer to the latter model as the "2D" model, and to the model with instantaneous synapses as the "1D" model.

As demonstrated in chapter 4, the response properties of the model are strongly affected by the baseline level of input. Therefore, a reasonable model comparison of the 1D and 2D models requires setting baseline levels so that the models operate in similar firing regimes. To do this, we normalize the input parameters $\mu(t)$ and $\sigma^2(t)$ such that the mean and variance of the voltage distributions will be the same for the two models, in the absence of spiking (no threshold or reset). We note that without threshold, the equations (5.1)-(5.3) are linear in the input $S(t)$. Using $S(t) = \delta(t)$, we find that the impulse voltage response for the 1D model is $v_{1D}(t) = \frac{R\overline{Q}}{\tau_m} e^{-t/\tau_m}$. For the 2D model, the current impulse response is $f(t) = \frac{\overline{Q}}{\tau_s} e^{-t/\tau_s}$, which leads to a voltage impulse $v_{2D}(t) = \frac{R\overline{Q}}{(\tau_m - \tau_s)} \left(e^{-t/\tau_m} - e^{-t/\tau_s} \right)$ where we have assumed $\tau_m > \tau_s$.

With these impulse responses, we can write the voltage response in integral form:

$$V(t) = V_L + v * S(t) = V_L + \int_{-\infty}^{0} S(t')v(t - t')dt', \tag{5.4}$$

where $*$ denotes convolution and v is the voltage impulse response. Now let $S(t) = \mu_s(t) + \sigma_s(t)\eta(t)$ be a white noise process with drift. Since the mean of a weighted sum of stochastic variables is the sum of the weighted means, we have

$$\mu_V(t) = V_L + \int_{-\infty}^{0} \mu_s(t')v(t - t')dt' = V_L + v * \mu_s(t). \tag{5.5}$$

Similarly, for independent random variables, the variance of the weighted sum is the sum of variances, weighted by the square of the original weighting factors. Therefore,

$$\sigma_V^2(t) = \int_{-\infty}^{0} \sigma_s^2(t')v^2(t - t')dt' = v^2 * \sigma_s^2(t). \tag{5.6}$$

We can use these equations to derive the mean and variance of the voltage distribution for baseline inputs having a constant mean μ_s and variance σ_s^2. For the 1D model,

$$\mu_V = \int_{-\infty}^{0} dt' \mu_s \frac{R\overline{Q}}{\tau_m} e^{-t'/\tau_m} = \mu_s R\overline{Q} \tag{5.7}$$

$$\sigma_V^2 = \int_{-\infty}^{0} dt' \sigma_s^2 \frac{R^2\overline{Q}^2}{\tau_m^2} e^{-2t'/\tau_m} = \sigma_s^2 \frac{R^2\overline{Q}^2}{2\tau_m}. \tag{5.8}$$

For the 2D model,

$$\mu_V = \int_{-infty}^{0} dt' \mu_s \frac{R\overline{Q}}{\tau_m - \tau_s} \left(e^{-t'/\tau_m} - e^{-t'/\tau_s} \right) = \mu_s R\overline{Q} \tag{5.9}$$

$$\sigma_V^2 = \int_{-\infty}^{0} dt' \sigma_s^2 \frac{R^2\overline{Q}^2}{(\tau_m - \tau_s)^2} \left(e^{-t'/\tau_m} - e^{-t'/\tau_s} \right)^2 = \sigma_s^2 \frac{R^2\overline{Q}^2}{2\left(\tau_m + \tau_s\right)}. \tag{5.10}$$

The same level of mean input, $\mu_{s1D} = \mu_{s2D}$, leads to the identical mean in the voltage distributions, $\mu_{V1D} = \mu_{V2D}$. To obtain the same variance of the voltage, $\sigma_{V1D}^2 = \sigma_{V2D}^2$ we set

$$\sigma_{s2D}^2 = \sigma_{s1D}^2 \frac{\tau_m + \tau_s}{\tau_m}. \tag{5.11}$$

5.3 Linear Response Properties

In this chapter, we make two distinct comparisons between the 1D and 2D LIF models. First, we compare the overall transfer function that takes time-varying input parameters to time-varying output firing rate. For small modulations in the input, this transformation will be linear and we let f be the linear filter converting input modulations to output rate modulations: $r(t) = (S * f)(t)$, where we abuse notation slightly by using $S(t)$ to denote modulation in the either input parameter, i.e. $S(t) = \mu_s(t)$ or $S(t) = \sigma_s^2(t)$. To characterize this transformation we take

Fourier transforms and apply the convolution theorem $[r](\omega) = [S][f](\omega)$, where we use $[Z](\omega)$ to denote the fourier transform of the function $Z(t)$. In practice, we use numerical simulations to obtain $[f](\omega) = [r](\omega)/[S](\omega)$. In all figures we normalize the gain by the baseline rates, i.e. we plot $[f](\omega)S_0/r_0$.

For the 2D model, we can view the transformation from input modulations to output rates as a two step process

$$S(t) \xrightarrow{f} r(t) = S(t) \xrightarrow{g} I(t) \xrightarrow{h} r(t). \tag{5.12}$$

The transformation g is the simple exponential filtering described by equation (5.3). Low gain at high frequencies for the 2D model may simply be due to the low-pass nature of the filtering from input to synaptic current, rather than a difference in the way the 1D and 2D models convert synaptic current to output spikes. To examine differences between the two models that are specific to this second transformation, we note that for small modulations, all of the transformations of equation (5.12) are linear with $f = h * g$. Again using the convolution theorem, we write $[h_{2D}](\omega) = [f_{2D}](\omega)/[g_{2D}](\omega)$. We then normalize this filter by baseline values and plot $([f_{2D}](\omega)/[g_{2D}](\omega))\,(I_0/r_0)$ where $I_0 = \overline{Q}\mu_{s0}$ for mean modulations and $I_0 = \frac{\overline{Q}^2\sigma_{s0}^2}{2\tau_s}$ for variance modulations.

5.4 Mean Perturbations

In this section, we compare the linear response dynamics of the 1D and 2D models in response to modulations in the mean input. Like the 1D model, the 2D LIF model displays low-pass filtering behavior to modulations in the mean input

rate (figures 5.1 and 5.2 left panels). However, the two filters display different phase behavior in the high-frequency limit, with phase shifts approaching $-45°$ for the 1D model, and $-180°$ in the 2D model.

Next we compare the two models after factoring out the direct effects of synaptic filtering in the 2D model (figure 5.1 middle and figure 5.2 middle). A major difference under this comparison is that the high-frequency gain is finite and flat for the 2D model, instead of decaying to zero as it does for the 1D model and for the full 2D model response. A second difference is that the overall filtering properties of the 2D model are regime dependent. In the Random Regime, the low-frequency gain is more than twice as large as the high-frequency gain for $\tau_s = 2$. As the baseline mean input values become even more sub-threshold (not pictured), the high-frequency gain becomes even smaller, suggesting that neurons in the Random Regime respond better to slow mean input changes. Here the response is practically low-pass as it is for the 1D model. Conversely, in the Regular Regime, the model acts all-pass and interestingly, the high-frequency gain can plateau at a level even higher than the low-frequency gain (figure 5.1 middle and figure 5.2 middle).

As for the 1D model, resonances for modulations in the mean input only occur in the Regular Regime where the model acts more like an oscillator (figure 5.1 bottom). The resonance peaks are smaller for the 2D model, and decrease with increasing τ_s. However, the bandwidth of the resonances is wider in the 2D model than in the 1D model.

Finally, the transformation from current to rate in the 2D model has much smaller phase shifts across frequency, and these approach zero at high frequencies.

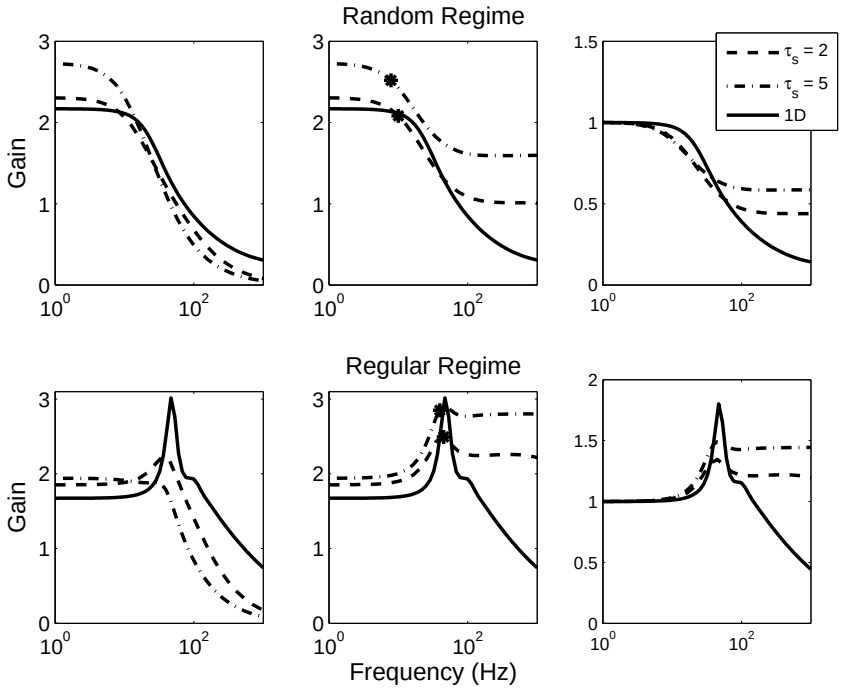

Figure 5.1: Gain curves for 2D model, $\tau_s = 2, 5$ and 1D model when the mean of the input is modulated. Top: Random Regime ($\mu_0 = 0.75\mu A/cm^2$ and $\sigma_0^2 = 3\mu A^2 msec/cm^4$); Bottom: Regular Regime ($\mu_0 = 1.5\mu A/cm^2$ and $\sigma_0^2 = 1\mu A^2 msec/cm^4$). Left: Full response; Middle: Response after accounting for current transformation; Right: Low-frequency response normalized to one.

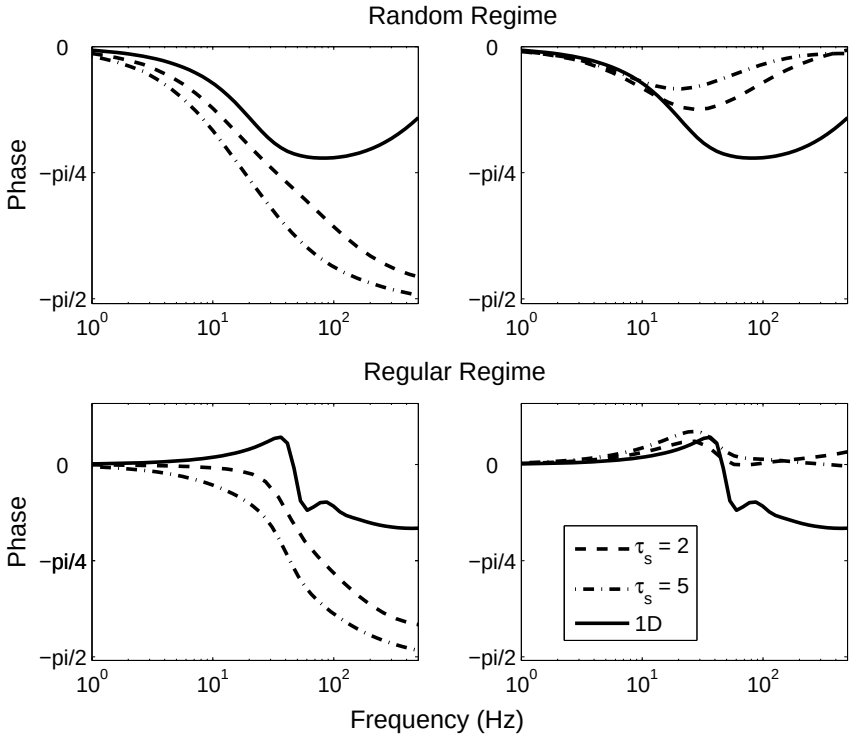

Figure 5.2: Phase curves for 2D model, $\tau_s = 2, 5$ and 1D model when the mean of the input is modulated. Top: Random Regime ($\mu_0 = 0.75\mu A/cm^2$ and $\sigma_0^2 = 3\mu A^2 msec/cm^4$); Bottom: Regular Regime ($\mu_0 = 1.5\mu A/cm^2$ and $\sigma_0^2 = 1\mu A^2 msec/cm^4$). Left: Full phase shift; Right: Phase shift after accounting for current transformation.

In contrast, high-frequency phase shifts go to $-45°$ for the 1D model and for the full 2D transformation. These results are in agreement with those found by Fourcaud and Brunel (2002), using a model where the mean-encoded modulations were not filtered through the synapse [Fourcaud and Brunel, 2002].

5.5 Variance Perturbations

Modulating the input variance reveals even greater differences in the behavior of the 1D and 2D models. The most obvious difference is the fact that amplitude of the entire gain curve is markedly reduced for the 2D model in the Regular Regime (figure 5.3 bottom). For very Regular baseline parameters, the high-frequency gain goes to zero for all values of τ_s (not shown). This result holds for the transformation from input current to firing rate, as well as for the full transformation from input rates to output rates. Therefore, this gain reduction is not simply due to the low-pass filtering of the input by the synaptic dynamics. Although not as extreme, the 2D model also shows a marked reduction in gain at high frequencies in the Random Regime (figure 5.3 top). Again, this effect persists even after dividing out the low-pass direct effect of synaptic filtering.

The resonance behavior of the 2D model is qualitatively similar to the 1D model. Resonances occur in both the Random and Regular Regimes, and the peak of the resonances occurs at frequencies that are higher than the steady-state firing rate with this difference increasing with increasing noise dominance (figure 5.3). We speculate that, similar to the 1D model, distinct mechanisms are responsible for

creating resonances to mean vs. variance modulations.

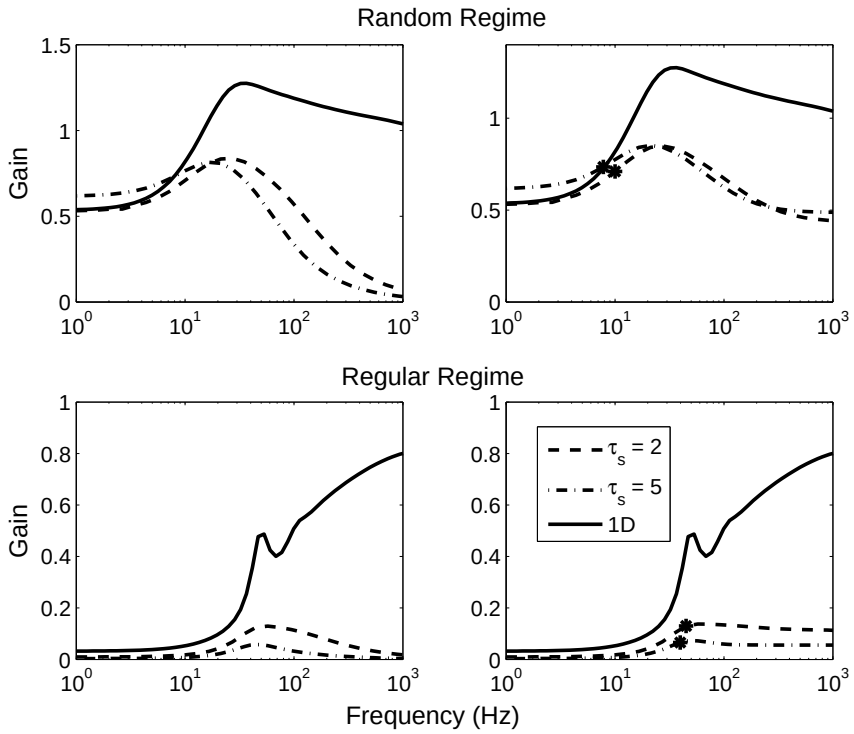

Figure 5.3: Gain curves for 2D model, $\tau_s = 2, 5$ and 1D model when the variance of the input is modulated. Top: Random Regime ($\mu_0 = 0.75\mu A/cm^2$ and $\sigma_0^2 = 3\mu A^2 msec/cm^4$); Bottom: Regular Regime ($\mu_0 = 1.5\mu A/cm^2$ and $\sigma_0^2 = 1\mu A^2 msec/cm^4$). Left: Full response; Right: Response after accounting for current transformation.

5.6 Discussion

Although many of the filtering properties of the 2D LIF model match those of the corresponding LIF model with instantaneous synapses, there are significant differences. As highlighted by Fourcaud and Brunel (2002), the synapses with finite

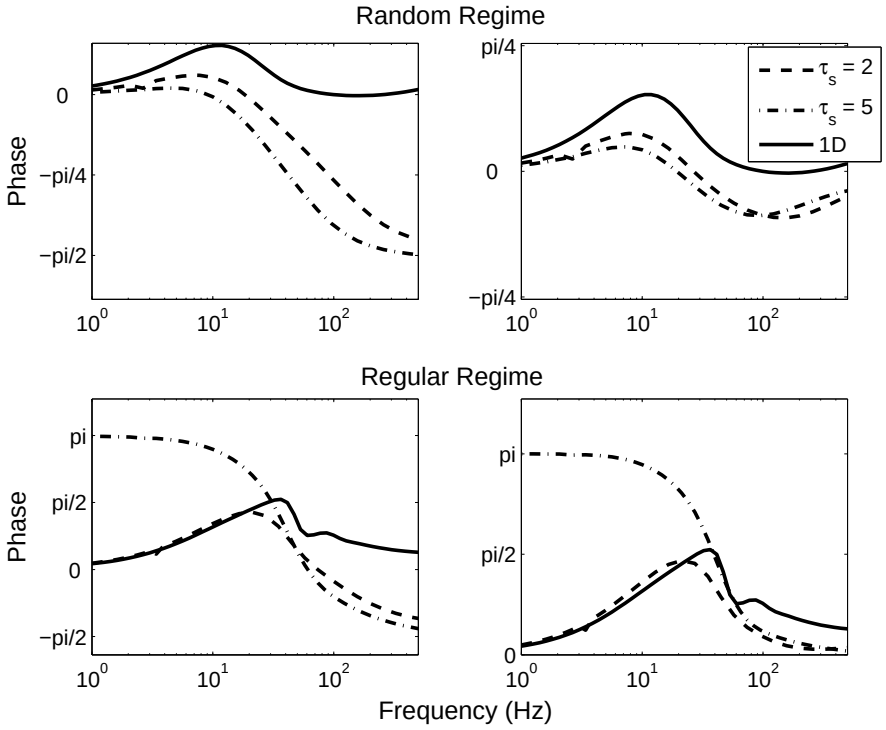

Figure 5.4: Phase curves for 2D model, $\tau_s = 2, 5$ and 1D model when the variance of the input is modulated. Top: Random Regime ($\mu_0 = 0.75\mu A/cm^2$ and $\sigma_0^2 = 3\mu A^2 msec/cm^4$); Bottom: Regular Regime ($\mu_0 = 1.5\mu A/cm^2$ and $\sigma_0^2 = 1\mu A^2 msec/cm^4$). Left: Full phase shift; Right: Phase shift after accounting for current transformation.

time constant in the 2D model lead to a finite high-frequency response to modulations in the mean [Brunel et al., 2001, Fourcaud and Brunel, 2002]. It also appears that the gain is flat across a range of high frequencies in the 2D model, independent of τ_s. Smaller values of τ_s are needed to confirm this conjecture. The difference in the high-frequency responses of the two models can be explained if we consider the two firing rate equations. For the 1D model, the mean only enters the firing rate equation through changes in the density of solutions lying with the boundary layer near threshold (4.5). Low-pass membrane filtering prevents changes in the mean from having immediate changes in the boundary layer and hence having any effect on the firing rate for high-frequency modulations. However, in the 2D model, the mean current is a component of the voltage flux and hence changes in the mean current have an immediate effect on the firing rate.

Here we show that the gain in response to variance modulations is reduced at high frequencies relative to the 1D model, and that there is a particularly large attenuation of the gain in the Regular Regime. In the Regular Regime, the suprathreshold mean input forces the membrane potential towards threshold and the model acts like an integrator [Lundstrom et al., 2008]. The variance has little affect on the baseline firing rate and we would expect that small changes in the variance would also evoke little response. We conjecture that the large high-frequency response of the 1D model is due to the artificial boundary conditions imposed to prevent the flux from becoming infinite. Because of the zero density threshold condition, the firing rate equation becomes directly proportional the variance in the Regular Regime. We believe the boundary conditions overemphasize the influence

that the variance has on the firing rate. Furthermore, these qualitatively different results between models suggest that the behavior of the 2D model does not approach that of the 1D model as τ_s goes to zero. Future work endeavors to determine a 1D model that is the limit of the 2D model.

Chapter 6

Integrate-and-Fire Nonlinear Response

6.1 Introduction

In their 2003 work, Fourcaud-Trocmé et al formulated the exponential integrate-and-fire (EIF) neuron model, whose peri-threshold voltage dynamics more closely matched models containing an active sodium current [Fourcaud-Trocmé et al., 2003]. They investigated the response of the EIF and other related models to sinusoidal inputs of varying amplitude and claimed that the model was well-approximated by a linear low-pass filter, for a range of inputs. The claim of linearity was based only on the fact that at each frequency, the gain of the response was independent of the amplitude injected. To determine if the response of the EIF model continued to be linear for a broader range of inputs, we calculated the temporal response to square-wave currents constructed with a range of amplitudes and a range of baseline currents. In a linear model, the onset and offset responses should be identical except for the sign. Our basic finding is that onset responses show a slower initial response but more rapidly reach the new equilibrium rate. We also compared the onset and offset response of the EIF model to the responses of the leaky integrate-and-fire (LIF) model. Generally, the EIF and LIF showed similar response patterns. The one substantial difference was that onset responses of the EIF model showed a greater delay relative to the LIF model. Finally, in a fully linear system, the re-

sponse to a sum of inputs equals the sum of the responses to the individual inputs. To investigate this, we performed a Fourier analysis of the square-wave input and compared the resulting gain and phase calculated from the separate presentation of the component sinusoidal inputs. At higher frequencies, the gain for the square wave inputs was reduced relative to the sinusoids, while the phase of the response was remarkably similar across frequencies.

6.2 Results

To assess the nonlinear components of response, we focused on input currents, I(t), containing sharp onset and offset transients. In particular, the majority of our simulations used a 5 Hz square-wave input current. Initially, we compared the instantaneous firing rate of the model for the onset period and offset period, averaging 750,000 trials over bins of 1 msec. Figure 1A illustrates the histogram obtained from the EIF model for a baseline current of $0.25\mu A/cm^2$ and a 5 Hz square-wave input of $0.5\mu A/cm^2$ amplitude. If the response of the EIF was linear, the onset and offset response should have the same shape. However, the time course of these responses differs significantly (figure 1B). From these simulations, it appears that there are three stages of the response of EIF models to a transient step in input current. First, there is a period from one to several milliseconds in which the response to an onset transient is delayed. While rates do increase slightly during this period, the increase is slow. The response to the offset transient shows no such delay, and firing rate immediately shows a rapid decline. In the second stage, the

response to both onsets and offsets changes rapidly, accounting for roughly 80% or more of the total change in rate. For the offset response, there is no noticeable distinction between these first two stages. In the third stage, the change in rate slows and eventually asymptotes at the steady state firing rate corresponding to the new level of current. It appears that the transition into this third, slowly changing stage happens earlier in time for the offset responses, and these rates approach asymptote more gradually. The response pattern for the LIF model is similar (figure 1C). However, the onset response does not show a distinct delay phase. Rather, both onset and offset responses change smoothly from baseline, but the onset response changes with a smaller slope.

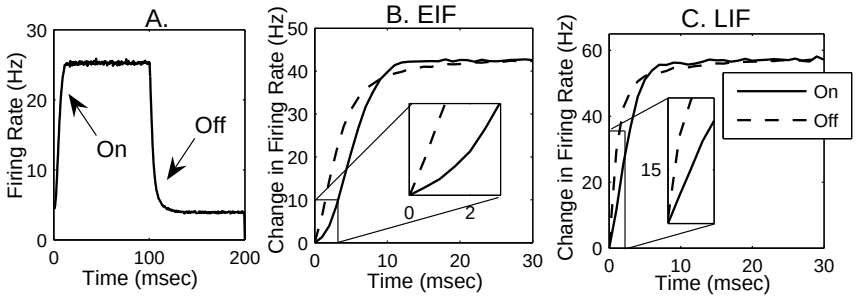

Figure 6.1: (A) The PSTH of the response of the EIF model to a square-wave input of $0.5\mu A/cm^2$ with a baseline current of $0.25\mu A/cm^2$. (B) The onset and offset responses are depicted together for comparison. Inset shows the first 3 msec of the response. (C) The onset and offset responses for the LIF model to a square-wave input of $0.5\mu A/cm^2$ and a baseline current of $0.25\mu A/cm^2$. Inset shows the first 2 msec of the response

6.2.1 Parameter Dependence - Qualitative Results

To characterize the dependence of the onset/offset difference on the amplitude of the input changes, we held the baseline current constant and varied the amplitude of the square-wave currents. As expected, for all baseline currents the difference between the onset and offset responses grew as the amplitude of the square-wave was increased. The case where $I_0 = 0.25\mu A/cm^2$ is delineated in figure 6.2A and 6.2C.

Next, we varied the baseline current while holding the amplitude of the square-wave current constant. Figure 6.2B and 6.2D depict the case where the baseline is $0.5\mu A/cm^2$ and the amplitude of the square-wave is varied from 0 to $0.5\mu A/cm^2$. The slopes of the initial response for the onset and offset differ less as the baseline current is increased. However, as the baseline current is increased, the neuron moves between the Random Regime, in which the mean current is sub-threshold and spikes are driven by random threshold crossings, and the Regular Regime in which the mean current is above threshold and the model produces regular trains of action potentials as the voltage is integrated up to threshold [Abeles, 1991, Troyer and Miller, 1997]. As the neuron moves into the Regular Regime, its response to a step change causes a predilection for spiking synchronously, creating an oscillation in the firing rate (figure 6.2B,D last box) [Gerstner, 2000]. It is unclear whether an over-damped version of this oscillation is related to the faster approach to the new firing rate demonstrated in the onset responses across the range of input parameters.

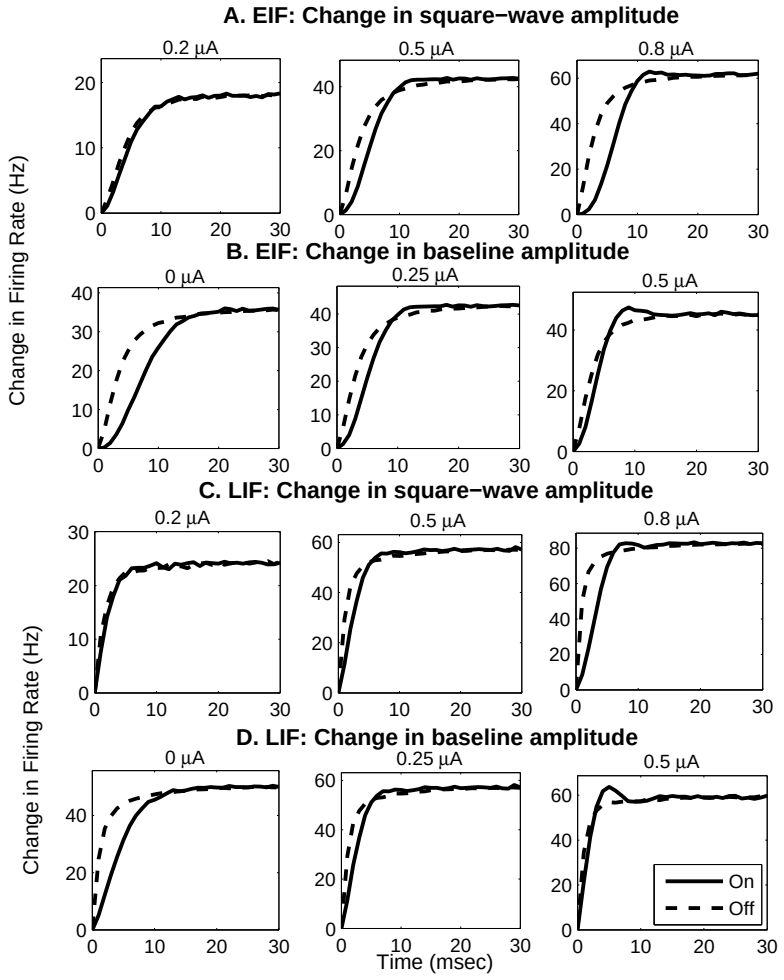

Figure 6.2: (A)The onset vs. offset responses for the baseline current $I_0 = 0.25\mu A/cm^2$. The amplitude of the square-wave is varied from 0.2 to $0.8\mu A/cm^2$. The difference in the onset and offset responses grows as the amplitude of the square-wave grows. (B) The onset vs. offset responses for square-wave current with amplitude $0.5\mu A/cm^2$ and baseline currents varying from 0.25 to $1\mu A/cm^2$. (C) Same as A except for the LIF instead of the EIF model. (D) Same as B except for the LIF instead of the EIF model.

6.2.2 Parameter Dependence - Quantitative Results

To more systematically examine how the response changes to changes in the amplitude and baseline of the input, we fit the onset and offset curves with the two-parameter hyperbolic ratio:

$$f(t) = \frac{t^n}{t^n + c^n}. \tag{6.1}$$

To enable the fit, we normalized the curves by dividing by the difference in equilibrium firing rates. The c parameter is most associated with the delay: time t equals c marks the time at which responses are midway between the new and old rates. The n parameter is associated with the steepness of the response, with a larger value of n meaning a steeper response function. When the regime starts switching to the Regular Regime, the response exhibits synchrony effects and this function no longer fits well. However, even though the function cannot fit the oscillations seen in this regime, it still fits the initial phases of the response, as well as doing a reasonable job of characterizing the overall approach to the new firing rate.

Figure 6.3 shows the values of the best-fit parameters as a function of square-wave amplitude for both low (dashed) and higher (solid) levels of the baseline current. The plots on the left show that increasing the amplitude affects the delay parameter c in opposite directions, increasing the delay for onset responses and reducing the delay for offset responses. Similar patterns are seen for high and low baseline simulations in both the EIF and LIF models, although high baseline currents and the LIF model are associated with lower delay overall. Increasing amplitude also causes an increasing difference in the steepness parameter n for both

the EIF and LIF models at high and low gain (right). However, unlike the delay parameter, changes in the steepness parameter are much more pronounced for the onset response; the offset response shows little change in n across parameters.

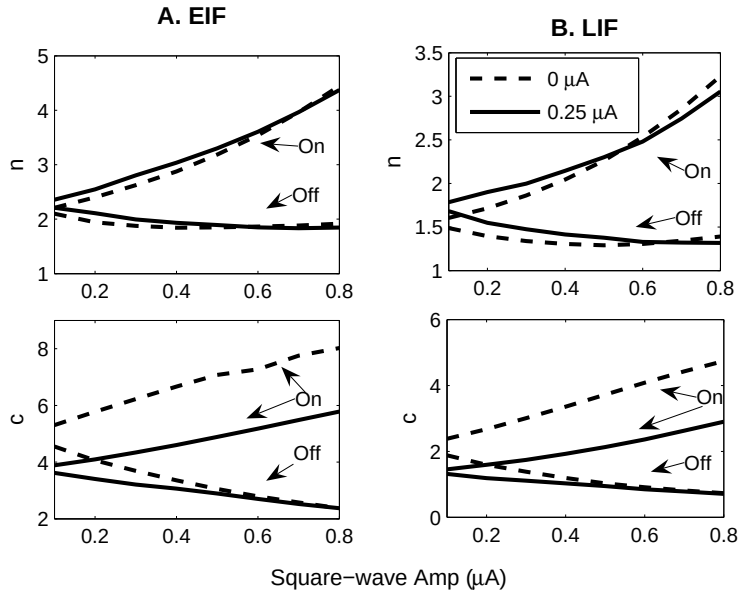

Figure 6.3: (A) The EIF model's onset and offset responses are fit with equation 6.1 and the parameters of f(t) are plotted for square-wave currents with amplitudes varying (x-axis) from 0.2 to 0.8. The parameters are plotted for $0\mu A/cm^2$ (dotted line) and $0.25\mu A/cm^2$ (solid line) baseline currents. (B) Same as A for the LIF model.

6.2.3 Fourier Analysis

Finally, we disassembled the square-wave input and resulting output into their Fourier components and calculated the gain and phase for each component. We then presented the sinusoidal components individually and calculated the gain and phase.

The comparison between the two calculations for a baseline current of $0\mu A/cm^2$ is shown in figure 6.4. For the model to act linearly, the response of the sums of inputs should be equal to the sum of the responses of the inputs. For low frequencies, the gain and phase for square-wave and sinusoidal inputs are very similar. But as the frequencies increase above approximately 40 Hz, the gains of the responses diverge. Near 100 Hz, the gain using the EIF model for square-wave inputs is nearly 25% lower than for the corresponding sinusoids and for the LIF model the gain is around 10% lower for the square-wave components. (The low gain found at higher frequencies resulted in less reliable measurements of gain and so these results are not shown.)

6.3 Discussion

Our results indicate that the temporal response of both the EIF and LIF models have a significant nonlinear component. In particular, offset transients have a more rapid onset followed by a slower decay as compared to onset transients. The difference between the onset and offset responses increases as the amplitude of the square-wave input is increased. Additionally, the gain due to the Fourier components of the square-wave response do not match the corresponding gain of the response to the sinusoids presented individually, especially for higher frequencies. With our parameters, the difference becomes pronounced above about 40 Hz. Although linear analyses can be a useful first step in characterizing the dynamic responses of model neurons, these results argue for a cautious interpretation of the results. More com-

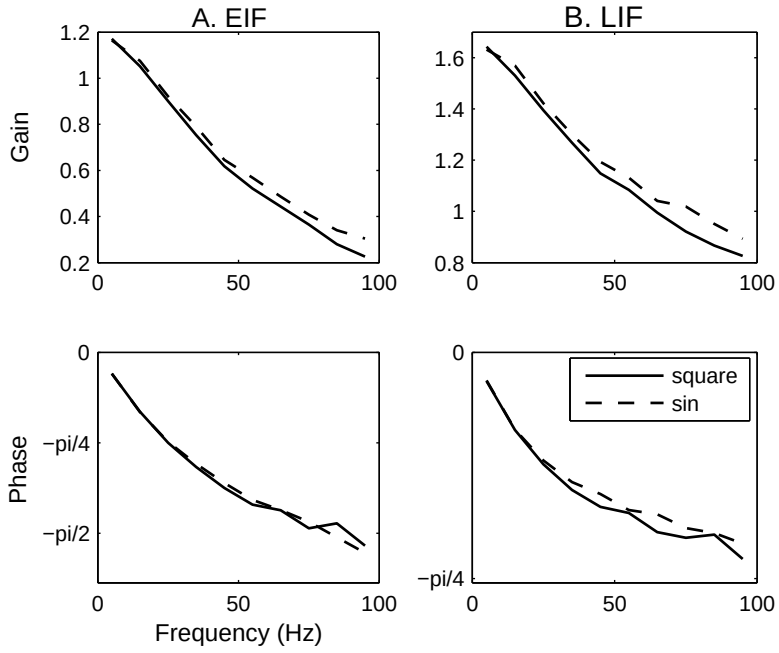

Figure 6.4: (A) The gain and phase of the EIF's response to the square-wave Fourier components and corresponding sinusoidal inputs for a baseline of $0\mu A/cm^2$ and a square-wave of $0.3\mu A/cm^2$. (B) Same as A for the LIF model.

plete characterizations will require a parametric exploration of the dynamic range over which the analysis is valid and/or an exploration of a wider range of stimuli than simple sinusoids.

Our study using square-wave inputs revealed three basic nonlinearities in the response of integrate-and-fire models. The most striking non-linearity is a delay in the onset response of the EIF model. This delay is not seen during offset responses or in either onset or offset responses of the LIF model. We speculate that this delay relates to time it takes for trajectories to travel from the voltage to infinity to be registered as a spike. The second basic nonlinearity is the slightly reduced slope in the rapidly changing phase of the response for onsets relative to offsets. In the LIF model, this is the main effect that makes the initial stage of onset responses slower than offset responses. Finally, a third nonlinearity is seen that results in offset responses returning more slowly to the new steady state firing rates than onset responses. Currently, it is unclear whether these different stages of the response should be considered distinct dynamical mechanisms, or whether they result from a single dynamical process unfolding over time.

Chapter 7

Conclusion

In this dissertation, we endeavored to delineate how the baseline pre-synaptic input values and the choice of encoding parameter (either the mean or variance of the input) affect neural response time. We also examined how including synaptic dynamics in the model alters the response dynamics. We focused on integrate-and-fire models (IF), since they are the simplest models of neuronal membrane dynamics that incorporate the essential features of signaling. Due to a simplifying approximation in the model of pre-synaptic input rates, we were able to study the response the using the Fokker-Planck framework [Ricciardi, 1977, Risken, 1989, Knight, 2000, Nykamp and Tranchina, 2000, Brunel, 2000, Fourcaud and Brunel, 2002].

We began by studying the response of the simplest IF model, the perfect integrate-and-fire model (PIF), which provides a good approximation of membrane dynamics when the mean input current is suprathreshold. Building on Knight's seminal work, which showed that the response of a population of PIF neurons is a scaled replica of a deterministic signal [Knight, 1972a], we used linear response theory to evaluate the response of the PIF to a stochastic signal. Fourcaud and Brunel have previously shown that the PIF acts like a low-pass filter for mean-encoded stochastic signals [Fourcaud and Brunel, 2002]. Following their derivation, we analytically solved for the linear response of the PIF to sinusoidal perturbations

in the variance. We found that the PIF acts like a high-pass filter when the variance was modulated. Moreover, variance perturbations elicit a response which is the exact compliment of the PIF response to the same size mean perturbations.

We exhibited that for the PIF, mean and variance perturbations elicit complimentary linear population responses. A common assumption is that pre-synaptic spike trains are Poisson distributed. Under this assumption, the mean and variance of the pre-synaptic rates will change proportionally. Therefore by perturbing the mean and variance concurrently, we found that the PIF response is a scaled replica of not only deterministic signals but of stochastic signals as well.

To survey neural response over a wider set of baseline mean input values, we next investigated the response properties of the leaky integrate-and-fire model (LIF), which better approximates membrane dynamics. Since the LIF is known to act very differently based on baseline input parameters values, we surveyed the response over a wide space, making sure to evaluate response for input parameters that put the model in qualitatively different response regimes. We did so for both mean and variance perturbations, to deduce how encoding the signal in the different parameters affected the response. Other researchers had provided partial results to this problem [Knight, 1972a, Lindner and Schimansky-Geier, 2001, Fourcaud and Brunel, 2002] but we strived to produce a compendium of LIF response.

We found that LIF response is dependent on both our choice of encoding parameter as well as the baseline input values. For variance perturbations, LIF filtering is regime dependent, all-pass in the Random Regime and high-pass in the Regular Regime. Because of this, we proposed a boundary between regimes based

on the low-frequency gain of the response due to variance perturbations.

When the signal was encoded in the variance, the high-frequency gain is equal to one, independent of baseline parameters. The finite high-frequency response to variance perturbations stems directly from the form of the firing rate equation, which is a product of two terms, the first of which is a weighted version of the variance and the second is a measure of the amount of trajectories near threshold. For high-frequency perturbations, the firing rate changes instantly due to the first term in the product, while the second term stays fixed.

Like the PIF, the LIF acts low-pass for mean perturbations [Brunel et al., 2001, Fourcaud and Brunel, 2002]. We showed that the cutoff frequency of the low-pass filter is systematically related to the steady-state firing rate. For the PIF, a natural cutoff frequency is the inverse of the time constant $\tau_e = \frac{\sigma_0^2}{2\mu_0^2}$. Future work will investigate how the cutoff frequency of the LIF is related to this new time constant.

Contrasting the PIF response to perturbations in the mean, the LIF shows resonances in the gain, as seen by Knight in his work using deterministic input [Knight, 1972a, Fourcaud and Brunel, 2002]. These resonances exist only in the Regular Regime and occurr at the steady-state firing rate, behavior expected from oscillatory mechanisms [Knight, 1972a, Brunel et al., 2001, Fourcaud and Brunel, 2002]. The addition of background noise reduces the size of the resonances. As for mean perturbations, variance perturbations elicit response resonances, but unexpectedly, resonances occurr in the Random Regime where firing is nonoscillatory. Resonances in the gain also occurr in the Regular Regime but as mean input decreases towards threshold, the resonances peak at frequencies much higher than the steady-state fir-

ing rate. For Random Regime resonances, the resonance peaks were also far above the steady-state firing rate.

We conjecture that there are two mechanisms that cause resonances when the signal is encoded in the variance. The first is the standard mechanism which causes resonances in oscillatory systems driven at their intrinsic frequency. The second mechanism may be solely responsible for Random Regime resonances and affect the placement of the peak of resonances when mean input is near threshold. Future work will analyze the dissected response, separating the flux due to drift and flux due to diffusion into separate terms and determine the response due to each term, trying to discover the mechanism behind Random Regime resonances.

Next we discussed how including synaptic dynamics in the model affected the response of the LIF. We included an equation for synaptic dynamics that represented the unbinding time course of neurotransmitter in the synapse [Brunel and Sergi, 1998, Haskell et al., 2001, Fourcaud and Brunel, 2002, Moreno-Bote and Parga, 2004]. We compared the 1D and 2D models using two measures. The 2D model exhibited low-pass filtering for both mean and variance perturbations, partly due to the low-pass synaptic filtering from input rates to synaptic current. To consider only the effect of the transformation from current to output firing rate, we used the convolutions that define the mean and variance of the current to divide out the effects of synaptic filtering. We found that under this reduced transformation, the LIF responds to arbitrarily fast modulations in the mean, unlike the 1D model. Fourcaud and Brunel found similar results in a model where the background input was filtered through the synapse but the signaling input was directly injected into the neuron

[Fourcaud and Brunel, 2002]. We also found resonances still arise, but are decreased in size as τ_s increases. Furthermore, the resonances are wider than for the 1D model. For variance changes, the model responded as an all-pass filter, when in the Random Regime. Strikingly, for the Regular Regime, the gain of the response due to variance perturbations is highly attenuated for all frequencies, and goes to zero in the high-frequency limit. Neurons act like integrators in the Regular Regime, with mean input predominantly determining return time to threshold. Therefore, it makes sense that variance changes would not greatly affect the firing rate response and little gain should be observed.

There are two components of our results that suggest that the 1D model is not the limit of the 2D model as $\tau_s \to 0$. First, in the Regular Regime, all values of τ_s elicit a flat high-frequency response to gain perturbations, as opposed to the limiting zero response of the 1D model. Additionally, the markedly reduced gain in the response due to variance perturbations suggests that the boundary conditions in the 1D model overemphasize the role of the noise. It remains to be seen, if these results will hold as the response is analyzed for values of τ_s much closer to zero. In the 1D model, the threshold boundary condition ($\rho = 0$) was imposed to prevent the flux from becoming infinite, which is a direct result of the white noise assumption. We endeavor to discover boundary conditions that better approximate the flow of trajectories over threshold, while keeping the model unidimensional. To do so, we will have to alter our assumptions about the nature of the stochastic input, at least in the boundary layer near threshold.

Finally, as a first step to understanding the full nonlinear response of neurons,

we studied the time course of onset and offset responses to transient inputs. We found that two IF models, although they behave slightly differently, both show offset responses with a steeper initial slope, but a slower approach to equilibrium than onset. Since these results exhibit nonlinearities in the response for realistic input parameter values, we wonder how the nonlinearities affect the full response to time-varying inputs. A future goal is to develop a better understanding of the essential aspects of the nonlinear response of IF models and construct a reduced model that incorporates these features as well as the linear features we have studied here.

Our work provides a stepping stone for understanding the response of network models composed of noisy neurons. We have shown that special care must be taken to choose proper parameters to transmit signals between the nodes of the network, with the input portraying the correct baseline and encoding mechanisms of the system.

Appendix A

Mathematical Formulations

A.1 Fokker-Planck Derivation

The following is a derivation of the 1D Fokker-Planck equation. It follows a general derivation from An Introduction to the Theory of Random Processes [Gikman and Skorokhod, 1965]. We will need the Chapman-Kolmogorov equation (CK):

$$\rho(y,s;x,t) = \int_{-\infty}^{\infty} \rho(y,s;z,u)\rho(z,u;x,t)dz, \quad t < u < s, \tag{A.1}$$

where ρ is the transition probability density function. The CK equation says that the pdf of transitioning from x to y from times t to s can be expressed as the sum over all the paths from x to z from times t to u and then from z to y in times u to s.

We will also use the following identity:

$$1 = \int_{-\infty}^{\infty} \rho(z,t;x,t-\Delta t)dz, \quad \Delta t > 0. \tag{A.2}$$

To begin the derivation, assume the membrane voltage follows a diffusion process, V, which satisfies 3 conditions:

1. Large changes in short amounts of time are improbable

2. A well-definied function exists for the infinitesimal mean (the drift term), $\frac{f(V)}{\tau_m}$

3. A well-definied function exists for the infinitesimal variance (the diffusion

term), $\frac{R^2\sigma^2}{\tau_m^2}$.

As an example, for the LIF:

$$f(V) = V_L - V + R\mu(t). \tag{A.3}$$

The drift and diffusion terms are determined from the SDE, equation (2.10). Mathematically the assumptions are:

$$\lim_{\Delta t\to 0^+} \frac{1}{\Delta t}\int_{|y-V|>\epsilon} \rho(y, t+\Delta t; V, t)dy = 0 \tag{A.4}$$

$$\lim_{\Delta t\to 0^+} \frac{1}{\Delta t}\int_{|y-V|\leq\epsilon} (y-V)\rho(y, t+\Delta t; V, t)dy = \frac{f(V)}{\tau_m} \tag{A.5}$$

$$\lim_{\Delta t\to 0^+} \frac{1}{\Delta t}\int_{|y-V|\leq\epsilon} (y-V)^2\rho(y, t+\Delta t; V, t)dy = \frac{R^2\sigma^2}{\tau_m^2}. \tag{A.6}$$

Note, all higher order moments are assumed to be zero.

Assume also, that there exist continuous partial derivatives of the transition pdf: $\frac{\partial\rho(y,s;x,t)}{ds}$, $\frac{\partial}{dV}[\frac{f(V)}{\tau_m}\rho(y,s;x,t)]$, and $\frac{\partial^2}{dV^2}[\frac{R^2\sigma^2}{\tau_m^2}\rho(y,s;x,t)]$.

Then, let $h \in C^3((-\infty,\infty))$ be a test function where, $h(x) = 0$ for $V \notin [A,B], h(A) = 0 = h(B)$ and $h'(A) = 0 = h'(B)$. For any A and B satisfying $-\infty < A < B < \infty$,

$$\int_{-\infty}^{\infty} h(y)\frac{\partial\rho(y,s;x,t)}{\partial s}dy = \frac{\partial}{\partial s}\int_{-\infty}^{\infty} h(y)\rho(y,s;x,t)dy \tag{A.7}$$

$$= \lim_{\Delta t\to 0}\frac{1}{\Delta t}\int_{-\infty}^{\infty} h(y)[\rho(y,s+\Delta t;x,t) - \rho(y,s;x,t)]dy. \tag{A.8}$$

Apply the Chapman-Kolmogorov equations to (A.8) and get

$$= \lim_{\Delta t\to 0}\frac{1}{\Delta t}\left[\int_{-\infty}^{\infty} h(y)\int_{-\infty}^{\infty}\rho(V,s;x,t)\rho(y,s+\Delta t;V,s)dV\,dy - \int_{-\infty}^{\infty} h(V)\rho(V,s;x,t)dV\right]. \tag{A.9}$$

Then change the order of integration and apply equation (A.2):

$$= \lim_{\Delta t \to 0} \left[\frac{1}{\Delta t} \int_{-\infty}^{\infty} \rho(V, s; x, t) \int_{-\infty}^{\infty} \rho(y, s + \Delta t; V, s)[h(y) - h(V)] dy dV \right]. \quad \text{(A.10)}$$

Then we expand h(y) about V:

$$= \lim_{\Delta t \to 0} \frac{1}{\Delta t} [\int_{-\infty}^{\infty} \rho(V, s; x, t) \int_{-\infty}^{\infty} \rho(y, s + \Delta t; V, s)[(y - V)h'(V) + \frac{(y - V)^2}{2} h''(V) + \frac{(y - V)^3}{6} h'''(\xi)] dy dV]. \quad \text{(A.11)}$$

Apply the assumptions for our diffusion process, equations (A.4) to (A.6):

$$= \int_{-\infty}^{\infty} \rho(V, s; x, t) \left[\frac{f(V)}{\tau_m} h'(V) + \frac{1}{2} \frac{R^2 \sigma^2}{\tau_m^2} h''(V) \right] dV. \quad \text{(A.12)}$$

Integrate each term by parts (the second one twice) and apply the assumptions about h(y), which makes all terms multiplied by h(y) evaluated at ∞ or $-\infty$ equal zero:

$$\int_{-\infty}^{\infty} \rho(V, s; x, t) \frac{f(V)}{\tau_m} h'(V) dV = - \int_{-\infty}^{\infty} h(V) \frac{\partial}{\partial V} \left[\frac{f(V)}{\tau_m} \rho(V, s; x, t) \right] dV \quad \text{(A.13)}$$

$$\int_{-\infty}^{\infty} \rho(V, s; x, t) \frac{1}{2} \frac{R^2 \sigma^2}{\tau_m^2} h''(V) dV = \int_{-\infty}^{\infty} h(V) \frac{\partial^2}{\partial V^2} \left[\frac{1}{2} \frac{R^2 \sigma^2}{\tau_m^2} \rho(V, s; x, t) \right] dV. \quad \text{(A.14)}$$

Substitute the preceding terms back into equation (A.12):

$$\int_{-\infty}^{\infty} h(V) \frac{\partial \rho(V, s; x, t)}{\partial t} dV = - \int_{-\infty}^{\infty} h(V) \frac{\partial}{\partial V} \left[\frac{f(V)}{\tau_m} \rho(V, s; x, t) \right] dV + \int_{-\infty}^{\infty} h(V) \frac{\partial^2}{\partial V^2} \left[\frac{1}{2} \frac{R^2 \sigma^2}{\tau_m^2} \rho(V, s; x, t) \right] dV. \quad \text{(A.15)}$$

And since we started with equation (A.7):

$$0 = \int_{-\infty}^{\infty} h(V) \left[\frac{\partial \rho(V,s;x,t)}{\partial t} + \frac{\partial}{\partial V} \left[\frac{f(V)}{\tau_m} \rho(V,s;x,t) \right] - \frac{\partial^2}{\partial V^2} \left[\frac{1}{2} \frac{R^2\sigma^2}{\tau_m^2} \rho(V,s;x,t) \right] \right] dV. \tag{A.16}$$

Since h is *any* test function:

$$\frac{\partial \rho(V,s;x,t)}{\partial t} = -\frac{1}{\tau_m} \frac{\partial [f(V)\rho(V,s;x,t)]}{\partial V} + \frac{1}{2} \frac{R^2\sigma^2}{\tau_m^2} \frac{\partial^2 \rho(V,s;x,t)}{\partial V^2}. \tag{A.17}$$

Letting $F_0(x)$ be the distribution function for this diffusion process at time = 0. We integrate equation (A.17) for $\rho(V,t;x,0)$ with respect to x. Then we arrive at the probability density function evolution equation, the Fokker-Planck equation, for the LIF with instantaneous synapses:

$$\tau_m \frac{\partial \rho(V,t)}{\partial (t)} = -\frac{\partial}{\partial V} [f(V)\rho(V,t)] + \frac{R^2\sigma^2}{2\tau_m} \frac{\partial^2 \rho(V,t)}{\partial V^2}. \tag{A.18}$$

A.2 PIF Solutions

A.2.1 Variance Perturbations

To determine the linear response of the PIF to perturbations in the mean of the input, we need to solve the 1st order nonhomogeneous ordinary differential equation:

$$i\tau_e \omega \widehat{\rho} = \frac{d^2\rho_0}{du^2} + \frac{d^2\widehat{\rho}}{du^2} - \frac{d\widehat{\rho}}{du}. \tag{A.19}$$

The boundary conditions for the 1st order equations are

$$\widehat{\rho}(u_\theta) = 0 \tag{A.20}$$

$$\widehat{\rho}(u_{r_+}) = \widehat{\rho}(u_{r_-}) \tag{A.21}$$

$$\left(\frac{\partial \rho_0}{\partial u}(u_\theta) + \frac{\partial \widehat{\rho}}{\partial u}(u_\theta, \omega)\right) = -r_0 \widehat{n}(\omega)\tau_e \tag{A.22}$$

$$\frac{\partial \rho_0}{\partial u}(u_{r_+}) - \frac{\partial \rho_0}{\partial u}(u_{r_-}) + \frac{\partial \widehat{\rho}}{\partial u}(u_{r_+}, \omega) - \frac{\partial \widehat{\rho}}{\partial u}(u_{r_-}, \omega) = -r_0 \widehat{n}(\omega)\tau_e \tag{A.23}$$

$$\int_{-\infty}^{\theta} \widehat{\rho}(u, \omega) du = 0. \tag{A.24}$$

In chapter 3 we showed that the general solution to equation (A.19) is

$$\widehat{\rho} = \frac{r_0}{i\omega}[-e^{u-u_\theta} + \Theta(u_r - u)(e^{u-ur})] +$$
$$Ce^{zp(u-u_\theta)} + D\Theta(u_r - u)e^{zp(u-u_r)} + Ee^{zn(u-u_\theta)} + F\Theta(u_r - u)e^{zn(u-u_r)}, \tag{A.25}$$

where $zp = z_+(\omega)$ and $zn = z_-(\omega)$ given by

$$z \pm (\omega) = \frac{1 \pm \sqrt{1 + 4i\omega\tau_e}}{2}. \tag{A.26}$$

F must equal zero else the density in boundary condition A.24 is not integrable because the modulus of the exponential multiplied by F will blow up.

Solving (A.20) for E:

$$-\frac{r_0}{i\omega} + C + E = 0 \tag{A.27}$$

$$E = \frac{r_0}{i\omega} - C. \tag{A.28}$$

Using the second boundary condition, equation (A.21), we solve for D:

$$-\frac{r_0}{i\omega} - D - F = 0 \tag{A.29}$$

$$D = -\frac{r_0}{i\omega}. \tag{A.30}$$

Equation (A.23) is used to solve for the 1st order response component $\widehat{n}(\omega)$:

$$-r_0\tau_e - \frac{r_0}{i\omega} - Dzp = -r_0\widehat{n}(\omega)\tau_e \tag{A.31}$$

$$\frac{-r_0\tau_e - \frac{r_0}{i\omega} + \frac{r_0}{i\omega}zp}{-r_0\tau_e} = \widehat{n}(\omega) \tag{A.32}$$

$$\widehat{n}(\omega) = 1 - \frac{\sqrt{1+4i\omega\tau_e}-1}{2i\omega\tau_e}. \tag{A.33}$$

Finally, we use equation (A.22) to solve for C:

$$-r_0\tau_e - \frac{r_0}{i\omega} + Czp + Ezn = -r_0\widehat{n}(\omega)\tau_e \tag{A.34}$$

$$-r_0\tau_e - \frac{r_0}{i\omega} + Czp + \left(\frac{r_0}{i\omega} - C\right)zn = -r_0\widehat{n}(\omega)\tau_e \tag{A.35}$$

$$C(zp - zn) = -r_0\left(\widehat{n}(\omega)\tau_e - \tau_e - \frac{1}{i\omega} + \frac{zn}{i\omega}\right) \tag{A.36}$$

$$C(\sqrt{1+4i\omega\tau_e}) = -r_0\left(-\frac{\sqrt{1+4i\omega\tau_e}-1}{2i\omega} - \frac{1}{i\omega} + \frac{1-\sqrt{1+4i\omega\tau_e}}{2i\omega}\right) \tag{A.37}$$

$$C = \frac{r_0}{i\omega}. \tag{A.38}$$

Therefore, the final solution is

$$\widehat{\rho} = \frac{r_0}{i\omega}[-e^{u-u_\theta} + \Theta(u_r - u)(e^{u-ur}) + e^{z_+(\omega)(u-u_\theta)} - \Theta(u_r - u)e^{z_+(\omega)(u-u_r)}] \tag{A.39}$$

A.2.2 Mean Perturbations

To determine the linear response of the PIF to perturbations in the variance of the input, we need to solve the 1st order nonhomogeneous ordinary differential equation:

$$i\tau_e\omega\widehat{\rho} = \frac{d^2\widehat{\rho}}{du^2} - \frac{d\widehat{\rho}}{du} - \frac{d\rho_0}{du}. \tag{A.40}$$

The boundary conditions for the 1st order equations are:

$$\widehat{\rho}(u_\theta) = 0 \tag{A.41}$$

$$\widehat{\rho}(u_{r_+}) = \widehat{\rho}(u_{r_-}) \tag{A.42}$$

$$\frac{\partial \widehat{\rho}}{\partial u}(u_\theta, \omega) = -r_0 \widehat{n}(\omega)\tau_e \tag{A.43}$$

$$\frac{\partial \widehat{\rho}}{\partial u}(u_{r_+}, \omega) - \frac{\partial \widehat{\rho}}{\partial u}(u_{r_-}, \omega) = -r_0 \widehat{n}(\omega)\tau_e \tag{A.44}$$

$$\int_{-\infty}^{\theta} \widehat{\rho}(u, \omega) du = 0. \tag{A.45}$$

In chapter 3 we showed that the general solution to equation (A.40) is

$$\widehat{\rho} = \frac{r_0}{i\omega}[e^{u-u_\theta} - \Theta(u_r - u)(e^{u-ur})] +$$
$$Ce^{zp(u-u_\theta)} + D\Theta(u_r - u)e^{zp(u-u_r)} + Ee^{zn(u-u_\theta)} + F\Theta(u_r - u)e^{zn(u-u_r)}, \tag{A.46}$$

where $zp = z_+(\omega)$ and $zn = z_-(\omega)$ given by

$$z \pm (\omega) = \frac{1 \pm \sqrt{1 + 4i\omega\tau_e}}{2}. \tag{A.47}$$

F must equal zero else the density in boundary condition A.45 is not integrable because the modulus of the exponential multiplied by F will blow up.

Solving (A.41) for E:

$$\frac{r_0}{i\omega} + C + E = 0 \tag{A.48}$$

$$E = -\frac{r_0}{i\omega} - C. \tag{A.49}$$

Using the second boundary condition, equation (A.42), we solve for D:

$$\frac{r_0}{i\omega} - D = 0 \tag{A.50}$$

$$D = \frac{r_0}{i\omega}. \tag{A.51}$$

Equation (A.44) is used to solve for the 1st order response component $\widehat{n}(\omega)$:

$$\frac{r_0}{i\omega} - Dzp = -r_0\widehat{n}(\omega)\tau_e \tag{A.52}$$

$$\frac{\frac{r_0}{i\omega} - \frac{r_0}{i\omega}zp}{-r_0\tau_e} = \widehat{n}(\omega) \tag{A.53}$$

$$\widehat{n}(\omega) = \frac{\sqrt{1+4i\omega\tau_e}-1}{2i\omega\tau_e}. \tag{A.54}$$

Finally, we use equation (A.43) to solve for C:

$$\frac{r_0}{i\omega} + Czp + Ezn = -r_0\widehat{n}(\omega)\tau_e \tag{A.55}$$

$$\frac{r_0}{i\omega} + Czp + \left(-\frac{r_0}{i\omega} - C\right)zn = -r_0\widehat{n}(\omega)\tau_e \tag{A.56}$$

$$C(zp - zn) = -r_0\left(\widehat{n}(\omega)\tau_e + \frac{1}{i\omega} - \frac{zn}{i\omega}\right) \tag{A.57}$$

$$C(\sqrt{1+4i\omega\tau_e}) = -r_0\left(\frac{\sqrt{1+4i\omega\tau_e}-1}{2i\omega} + \frac{1}{i\omega} - \frac{1-\sqrt{1+4i\omega\tau_e}}{2i\omega}\right) \tag{A.58}$$

$$C = \frac{-r_0}{i\omega}. \tag{A.59}$$

Therefore, the final solution is

$$\widehat{\rho} = \frac{r_0}{i\omega}[e^{u-u_\theta} - \Theta(u_r-u)(e^{u-ur}) - e^{z_+(\omega)(u-u_\theta)} + \Theta(u_r-u)e^{z_+(\omega)(u-u_r)}] \tag{A.60}$$

Bibliography

[Abbott, 1999] Abbott L. F. (1999). Lapicque's introduction of the integrate-and-fire model neuron (1907). *Brain Research Bulletin*, 50(5-6):303–304.

[Abbott and van Vreeswijk, 1993] Abbott L. F. and van Vreeswijk C. (1993). Asynchronous states in networks of pulse-coupled oscillators. *Physical Review E*, 48(2):1483–1490.

[Abeles, 1991] Abeles M. (1991). *Corticonics: Neural Circuits of the Cerebral Cortex*. Cambridge University Press.

[Allen, 2003] Allen L. J. S. (2003). *An Introduction to Stochastic Processes with Applitcations to Biology*. Pearson Prentice Hall, Upper Saddle River, NJ.

[Arnold, 1974] Arnold L. (1974). *Stochastic Differential Equations*. John Wiley & Sons, Inc., New York.

[Barak and Tsodyks, 2006] Barak O. and Tsodyks M. (2006). Recognition by variance: learning rules for spatiotemporal patterns. *Neural Computation*, 18(10):2343–2358.

[Brunel, 2000] Brunel N. (2000). Dynamics of sparsely connected networks of excitatory and inhibitory spiking neurons. *Journal of Computational Neuroscience*, 8(3):183–208.

[Brunel et al., 2001] Brunel N., Chance F. S., Fourcaud N., and Abbott L. F. (2001). Effects of synaptic noise and filtering on the frequency response of spiking neurons. *Physical Review Letters*, 86(10):2186–2189.

[Brunel and Hakim, 1999] Brunel N. and Hakim V. (1999). Fast global oscillations in networks of integrate-and-fire neurons with low firing rates. *Neural Computation*, 11(7):1621–1671.

[Brunel and Sergi, 1998] Brunel N. and Sergi S. (1998). Firing frequency of leaky intergrate-and-fire neurons with synaptic current dynamics. *Journal of Theoretical Biology*, 195(1):87–95.

[Bulsara et al., 1996] Bulsara A. R., Elston T. C., Doering C. R., Lowen S. B., and Lindenberg K. (1996). Cooperative behavior in periodically driven noisy integrate-fire models of neuronal dynamics. *Physical Review E*, 53(4):3958–3969.

[Burkitt, 2006a] Burkitt A. N. (2006a). A review of the integrate-and-fire neuron model: I. homogeneous synaptic input. *Biological Cybernetics*, 95(1):1–19.

[Burkitt, 2006b] Burkitt A. N. (2006b). A review of the integrate-and-fire neuron model: II. inhomogeneous synaptic input and network properties. *Biological Cybernetics*, 95(2):97–112.

[Destexhe et al., 1998] Destexhe A., Mainen Z.F., and Sejnowski T.J. (1998). *Kinetic models of synaptic transmission*, pages 1–25. MIT Press, Cambridge, MA.

[Fourcaud and Brunel, 2002] Fourcaud N. and Brunel N. (2002). Dynamics of the firing probability of noisy integrate-and-fire neurons. *Neural Computation*, 14(9):2057–2110.

[Fourcaud-Trocmé and Brunel, 2005] Fourcaud-Trocmé N. and Brunel N. (2005). Dynamics of the instantaneous firing rate in response to changes in input statistics. *Journal of Computational Neuroscience*, 18(3):311–321.

[Fourcaud-Trocmé et al., 2003] Fourcaud-Trocmé N., Hansel D., van Vreeswijk C., and Brunel N. (2003). How spike generation mechanisms determine the neuronal response to fluctuating inputs. *Journal of Neuroscience*, 23(37):11628–11640.

[Gammaitoni et al., 1998] Gammaitoni L., Hänggi P., Jung P., and Marchesoni F. (1998). Stochastic resonance. *Reviews of Modern Physics*, 70(1):223–287.

[Gerstein and Mandelbrot, 1964] Gerstein G. L. and Mandelbrot B. (1964). Random walk models for the spike activity of a single neuron. *Biophysical Journal*, 4:41–68.

[Gerstner, 2000] Gerstner W. (2000). Population dynamics of spiking neurons: fast transients, asynchronous states, and locking. *Neural Computation*, 12(1):43–89.

[Gikman and Skorokhod, 1965] Gikman I.I. and Skorokhod A.V. (1965). *Introduction to the Theory of Random Processes*. W. B. Saunders Company, Philadelphia, PA.

[Hansel and van Vreeswijk, 2002] Hansel D. and van Vreeswijk C. (2002). How noise contributes to contrast invariance of orientation tuning in cat visual cortex. *Journal of Neuroscience*, 22(12):5118–5128.

[Haskell et al., 2001] Haskell E., Nykamp D. Q., and Tranchina D. (2001). Population density methods for large-scale modelling of neuronal networks with realistic synaptic kinetics: cutting the dimension down to size. *Network*, 12(2):141–174.

[Hasselmo, 2005] Hasselmo M. E. (2005). What is the function of hippocampal theta rhythm?–linking behavioral data to phasic properties of field potential and unit recording data. *Hippocampus*, 15(7):936–949.

[Holt et al., 1997] Holt G., Koch C., Douglas R. J., and Mahowald M. (1997). The membrane time constant and firing rate dynamics. http://citeseer.ist.psu.edu/70702.html.

[Honeycutt, 1992] Honeycutt R. L. (1992). Stochastic runge-kutta algorithms. I. white noise. *Physical Review A*, 45(2):600–603.

[Hutcheon and Yarom, 2000] Hutcheon B. and Yarom Y. (2000). Resonance, oscillation and the intrinsic frequency preferences of neurons. *Trends in Neuroscience*, 23(5):216–222.

[Izhikevich, 2003] Izhikevich E. M. (2003). Simple model of spiking neurons. *IEEE Transactions of Neural Networks*, 14(6):1569–1572.

[Izhikevich, 2004] Izhikevich E. M. (2004). Which model to use for cortical spiking neurons? *IEEE Transactions on Neural Networks*, 15(5):1063–1070.

[Kandel et al., 2000] Kandel E.R., Schwartz J.H., and Jewell T.M. (2000). *Principles of Neural Science*. McGraw-Hill Medical.

[Knight, 1972a] Knight B. W. (1972a). Dynamics of encoding in a population of neurons. *Journal of General Physiology*, 59(6):734–766.

[Knight, 1972b] Knight B. W. (1972b). The relationship between the firing rate of a single neuron and the level of activity in a population of neurons. experimental evidence for resonant enhancement in the population response. *Journal of General Physiology*, 59(6):767–778.

[Knight, 2000] Knight B. W. (2000). Dynamics of encoding in neuron populations: some general mathematical features. *Neural Computation*, 12(3):473–518.

[Koene and Hasselmo, 2005] Koene R. A. and Hasselmo M. E. (2005). An integrate-and-fire model of prefrontal cortex neuronal activity during performance of goal-directed decision making. *Cerebral Cortex*, 15(12):1964–1981.

[Lánský and Sacerdote, 2001] Lánský P. and Sacerdote L. (2001). The ornstein-uhlenbeck neuronal model with signal-dependent noise. *Physics Letters A*, 285:132–140.

[Larsson and Thomée, 2003] Larsson S. and Thomée V. (2003). *Partial Differential Equations with Numerical Methods*. Springer-Verlag, Heidelberg, Germany.

[Lindner and Schimansky-Geier, 2001] Lindner B. and Schimansky-Geier L. (2001). Transmission of noise coded versus additive signals through a neuronal ensemble. *Physical Review Letters*, 86(14):2934–2937.

[Lundstrom et al., 2008] Lundstrom B. N., Hong S., Higgs M. H., and Fairhall A. L. (2008). Two computational regimes of a single-compartment neuron separated by a planar boundary in conductance space. *Neural Computation*, 20(5):1239–1260.

[Moreno-Bote and Parga, 2004] Moreno-Bote R. and Parga N. (2004). Role of synaptic filtering on the firing response of simple model neurons. *Physical Review Letters*, 92(2):028102.

[Naundorf et al., 2005] Naundorf B., Geisel T., and Wolf F. (2005). Action potential onset dynamics and the response speed of neuronal populations. *Journal of Computational Neuroscience*, 18(3):297–309.

[Nykamp and Tranchina, 2000] Nykamp D. Q. and Tranchina D. (2000). A population density approach that facilitates large-scale modeling of neural networks: analysis and an application to orientation tuning. *Journal of Computational Neuroscience*, 8(1):19–50.

[Omurtag et al., 2000] Omurtag A., Knight B. W., and Sirovich L. (2000). On the simulation of large populations of neurons. *Journal of Computational Neuroscience*, 8(1):51–63.

[Plesser and Geisel, 1999] Plesser H. E. and Geisel T. (1999). Markov analysis of stochastic resonance in a periodically driven integrate-and-fire neuron. *Physical Review E*, 59(6):7008–7017.

[Plesser and Geisel, 2001] Plesser H. E. and Geisel T. (2001). Stochastic resonance in neuron models: endogenous stimulation revisited. *Physical Review E*, 63(3 Pt 1):031916.

[Plesser and Gerstner, 2000] Plesser H. E. and Gerstner W. (2000). Noise in integrate-and-fire neurons: from stochastic input to escape rates. *Neural Computation*, 12(2):367–384.

[Pressley and Troyer, 2006] Pressley J. and Troyer T. W. (2006). Temporal processing in the exponential integrate-and-fire model is nonlinear. *Neurocomputing*, 69:1076–1080.

[Ricciardi, 1977] Ricciardi L. (1977). *Lecture Notes in Biomathematics*. Springer-Verlag, Heidelberg, Germany.

[Rieke et al., 1997] Rieke F. M., Warland D., de Ruyter van Steveninck R., and Bialek W. (1997). *Spikes: Exploring the Neural Code*. MIT Press, Cambridge, MA.

[Risken, 1989] Risken H. (1989). *The Fokker-Planck Equation: Methods of Solution and Application*. Springer-Verlag, Berlin, 2nd edition.

[Salinas and Sejnowski, 2002] Salinas E. and Sejnowski T. J. (2002). Integrate-and-fire neurons driven by correlated stochastic input. *Neural Computation*, 14(9):2111–2155.

[Shadlen and Newsome, 1994] Shadlen M. N. and Newsome W. T. (1994). Noise, neural codes and cortical organization. *Current Opinion in Neurobiology*, 4(4):569–579.

[Silberberg et al., 2004] Silberberg G., Bethge M., Markram H., Pawelzik K., and Tsodyks M. (2004). Dynamics of population rate codes in ensembles of neocortical neurons. *Journal of Neurophysiology*, 91(2):704–709.

[Softky and Koch, 1993] Softky W. R. and Koch C. (1993). The highly irregular firing of cortical cells is inconsistent with temporal integration of random epsps. *Journal of Neuroscience*, 13(1):334–350.

[Troyer and Miller, 1997] Troyer T. W. and Miller K. D. (1997). Physiological gain leads to high isi variability in a simple model of a cortical regular spiking cell. *Neural Computation*, 9(5):971–983.

[Tuckwell, 1988] Tuckwell H. C. (1988). *Introduction to Theoretical Neurobiology: Volume 2*. Cambridge University Press.

[Vreugdenshil, 1989] Vreugdenshil C.B. (1989). *Computational Hydraulics*. Springer-Verlag, Berlin.

[Wilson and Cowan, 1973] Wilson H. R. and Cowan J. D. (1973). A mathematical theory of the functional dynamics of cortical and thalamic nervous tissue. *Kybernetik*, 13(2):55–80.